Phase transitions and shapes of two component membranes and vesicles II : weak segregation limit

Takashi Taniguchi ([1]), Kyozi Kawasaki ([1]), David Andelman ([2, 3]) and Toshihiro Kawakatsu ([1])

([1]) Department of Physics, Kyushu University 33, Fukuoka 812, Japan
([2]) School of Physics and Astronomy, Raymond and Beverly Sackler Faculty of Exact Sciences, Tel-Aviv University, Ramat Aviv 69978, Tel Aviv, Israel
([3]) Laboratoire P.S.I., Section Physique et Chimie, Institut Curie, 11 rue P. et M. Curie, 75231 Paris Cedex 05, France

Abstract. — We investigate equilibrium shapes of vesicles composed of a mixture of partially miscible amphiphiles embedded in two- and three-dimensional space. The amphiphilic molecules can diffuse within the membrane and undergo an intramembrane phase separation below a critical temperature. We assume a simple phenomenological coupling between the local relative composition of the amphiphiles and the local curvature of the membrane shape. A linear stability analysis in the vicinity of the critical temperature indicates that a shape instability is induced by the coupling. Using a single mode approximation, we obtained phase diagrams for : (i) two-dimensional vesicles and (ii) three-dimensional axisymmetric vesicles. The equilibrium shape deformations are shown to depend on the phenomenological parameters of our model yielding highly non-trivial vesicle shapes which deviate from spherical-like objects.

1. Introduction.

Amphiphilic molecules in aqueous solution often self-assemble as bilayer membranes. Those membranes can form closed objects known as *vesicles* (liposomes) exhibiting a wide variety of shapes. Recent theoretical studies using an elastic continuum model have been quite successful in explaining the shape deformations of real biomembranes such as the biconcave shape of *erythrocytes* [1-4]. However, in these works, the membranes are treated as structureless and homogeneous layers, whereas, real biomembranes are heterogeneously composed of amphiphiles and intramembrane proteins that can freely diffuse within the membrane.

Motivated by the large complexity of real biomembranes, an increasing number of works have recently been devoted to studying shape deformations of membranes coupled to their internal degrees of freedom. Among others, these include the orientational order of the tilt angle of amphiphilic molecules with respect to the membrane plane [5], the dual network in erythrocyte membrane (the lipid/spectrin membrane) [6], the local density of amphiphilic molecules on the membrane in order to explain the phase transition from L_α or L_β phase to P_β phase [7], and the intramembrane phase separation of mixtures of amphiphiles [8-18]. In

addition, computer simulations of two-dimensional vesicles using a microscopic model regarding amphiphilic molecules as rigid rods (or rigid wedges) have been performed [19].

Let us consider the case of a mixed membrane, composed of two types of amphiphiles, as an example of a membrane with an additional inplane degree of freedom. Experimentally, it is known that a lateral phase separation can occur in such a mixed membrane [20]. It has been reported [21] that the *crenated* shapes (the *echinocytosis*) of red blood cells are induced by either anionic or non-ionic amphiphiles which are intercalated from the solution into the membrane, while cationic amphiphiles give rise to the phenomenon of *invagination*. It has been proposed [22] that an asymmetric distribution of intercalated amphiphilic lipids between the two layers of the membrane is at the origin of the crenated and invaginated shape deformations. Anionic amphiphiles are intercalated preferentially into the outer layer, while cationic ones are intercalated into the inner layer due to the interaction with the negatively charged lipid (phosphatidyl-serine) as they are usually concentrated in the inner layer of the erythrocyte membrane. Such intercalated compounds expand the area of one of the bilayers, resulting in crenation or invagination. This effect of asymmetrically distributed « impurities » (different kinds of amphiphiles from original constituents) between the outer and the inner layers has also been considered theoretically [7-18]. A coupling between the local curvature of the membrane and the local concentration of intercalated « impurities » can induce both an inhomogeneous distribution of impurities and a local shape deformation.

In the present work, shape deformations of vesicles composed of two amphiphiles, A and B, are investigated as well within a coupling between local composition and curvature. We consider here only the *weak* A/B segregation limit which is valid in the vicinity of a critical point. This complements our previous studies [10, 12], where the other limit of strong segregation between the two amphiphiles was investigated. The organization of this paper is as follows. In section 2, the general formalism of our phenomenological model is described in detail. We consider two-component vesicles embedded in two- and three-dimensional spaces. In section 3, shape deformations of two-dimensional vesicles or equivalently cylindrical vesicles are investigated in the vicinity of the critical point. In such a situation, both the amplitude of the shape deformation and the deviation of the local composition from its average value are small enough so that the free energy can be expanded in a power series in these small deviations. A linear stability analysis is performed, and an instability of the shape deformation is found to occur. Phase diagrams calculated within a single mode approximation are presented. In section 4, shape deformations of three-dimensional vesicles are studied, using again a linear stability analysis. In addition, phase diagrams are presented for axisymmetric vesicles. Finally, our concluding remarks are given in section 5.

2. General formalism.

Consider a closed-form membrane (vesicle) consisting of a lipid bilayer. Our formalism applies to two-dimensional (2d) vesicles represented by a closed contour in 2d space as well as to three-dimensional (3d) vesicles represented by a closed surface embedded in 3d space. In the former case, a 2d vesicle can also be thought of as a cross section of a cylindrical vesicle in 3d. We focus on shape deformations of vesicles having a simply-connected topology (circular like) in 2d and spherical-like (genus 0) in 3d. Fissions, fusions and other possible topological changes of vesicles will not be considered [23].

Symmetrical bilayer membranes (i.e., composed of two identical sides), or amphiphilic monolayers with no spontaneous curvature [24], are characterized by the following elastic energy [1]

$$\frac{\kappa}{2} \int H^2 \sqrt{g} \, d^D u \qquad (2.1)$$

where κ is the bending elasticity modulus [25], $\frac{1}{2} H$ the mean curvature, $D \equiv d - 1$, d being the dimensionality of the embedding space and $\sqrt{g}\ d^D u$ is the line (area) element in 2d (3d) (see Appendix A for more technical details). The integrals in equation (2.1) and hereafter are performed over the entire contour (2d) or surface (3d) of the vesicle. For 3d systems, the Gaussian curvature should be added, in general, to equation (2.1). Since we focus on vesicles with spherical topology (genus 0), this term adds only a constant contribution to the free energy due to Gauss-Bonnet Theorem [26] and can be ignored [25].

So far ideal structureless membranes are described. However, real biological membranes are composed of several different types of amphiphiles, intramembrane proteins and other molecules. Phospholipids and other substances intercalated into the outer and inner layers can diffuse within the membrane [20]. For simplicity, let us suppose that the membrane is composed of two different types of amphiphiles (A and B species). Such a mixed A/B membrane can undergo a lateral phase separation below a critical temperature [20]. Motivated by the slow rate of inside-outside (« flip-flop ») transition [27], we will, for simplicity, entirely neglect exchanges of amphiphilic molecules between the inner and outer layers of the membrane. The phase separation can be described by an order parameter $\Phi = \Phi_A - \Phi_B$ being the relative concentration per unit area. Close to the critical point, a Ginzburg-Landau expansion of the free energy in powers of Φ yields

$$\left.\begin{array}{l} F_2 = \int \left\{ \dfrac{b}{2} (\nabla \Phi)^2 + f(\Phi) \right\} \sqrt{g}\ d^D u \\[1.2em] f(\Phi) = -\mu \Phi + \dfrac{A_2}{2!} \Phi^2 + \dfrac{A_3}{3!} \Phi^3 + \dfrac{A_4}{4!} \Phi^4 \end{array}\right\} \qquad (2.2)$$

where b and A_i ($i = 2$, 3 and 4) are constant coefficients, and μ denotes the chemical potential difference between the A and B species. We included odd powers in Φ in the expansion (2.2) to account for the more general case where the system is composed of two different amphiphiles and is not, in general, symmetric about $\Phi = 0$. Such a free energy functional models two component membranes which undergo a *fluid/fluid* phase separation, while most experiments are performed in a *fluid/gel* coexistence region. Experiments on systems undergoing fluid/fluid phase separation are therefore necessary to check the validity of the present theory.

In the case where an amphiphilic monolayer is composed of an A/B mixture with different spontaneous curvatures [28], such a monolayer prefers curved morphologies depending on the A/B composition. The spontaneous curvature coming from the spatial inhomogeneity of the relative concentration Φ can be modeled by the following phenomenological coupling between composition and mean curvature [8, 9]

$$\Lambda \int \Phi H \sqrt{g}\ d^D u \qquad (2.3)$$

where Λ is a coupling constant. The coupling mechanism which appeared in equation (2.3) can also be applied to mixed bilayer membranes [7]. Asymmetric distribution of the absorbed substance (e.g., anionic, non-ionic or cationic amphiphiles) between the outer and inner layers may cause a local spontaneous curvature. As was mentioned above, anionic and non-ionic amphiphiles are preferentially absorbed from solution onto the outer layer of erythrocytes causing a crenated shape (echinocytosis). On the other hand, cationic amphiphiles are absorbed onto the inner layer causing an invaginated shape [21, 22].

We introduce a pressure difference ($P = P_{out} - P_{in}$) across the vesicle and add a term PV (in 3d) or PA (in 2d) to the total free energy. One can choose either a fixed pressure

constraint or a fixed volume constraint in 3d (a fixed area constraint in 2d). For the fixed volume constraint, the pressure difference acts as a Lagrange multiplier which guarantees the specified value of the total interior volume (area in 2d) of the vesicle. In investigating fluctuations of an equilibrium shape of a vesicle, the fixed volume and the fixed pressure constraints can be read as V- and P-ensembles, respectively [29]. The V-ensemble is suitable to describe short time behavior such as the erythrocyte flickering phenomenon, in which the volume of vesicle does not change. On the other hand, the P-ensemble is more suitable to describe the long time behavior. In the latter case, the solvent can diffuse across the vesicular membrane, causing changes in the enclosed volume [30]. The difference between those two constraints is important in the investigations on the dynamics of vesicles as well as on the fluctuations in the equilibrium state. The difference between phase diagrams under the fixed pressure constraint and under the fixed volume constraint are discussed in reference [17]. In the present paper, we use the fixed pressure constraint. Such a constraint is suitable to describe equilibrium states under an imposed pressure in the long time regime as well as it simplifies the calculation.

The equilibrium state of the vesicle is determined by minimizing the total free energy under the following two constraints.

(a) The membrane is incompressible. Namely, the total surface area of vesicles (total contour length in 2d) is fixed.

$$\int \sqrt{g}\, \mathrm{d}^D u = \begin{cases} L & \text{in} \quad 2d \\ S & \text{in} \quad 3d \end{cases} \tag{2.4}$$

where $L(S)$ is the fixed total contour length (total area) of the vesicle.

(b) The total amount of amphiphiles on the vesicle is also conserved. Namely, we assume that amphiphiles on the vesicle do not exchange with an external reservoir. For amphiphilic monolayer, this means that the total amount of amphiphiles in the layer is conserved. The area (line in 2d) fraction of A and B species in the layer is specified by

$$\int \Phi \sqrt{g}\, \mathrm{d}^D u = \begin{cases} \langle \Phi \rangle\, L & \text{in} \quad 2d \\ \langle \Phi \rangle\, S & \text{in} \quad 3d \end{cases} \tag{2.5}$$

where equation (2.5) expresses the difference between the amount of A and B in the monolayer and $\langle \Phi \rangle$ denotes the average of the order parameter. The constraint equation (2.5) is also applicable to bilayer membranes if the outer layer is composed of the A and the B amphiphiles while the inner layer consists only of the A amphiphiles. Since the amphiphiles are assumed not to flip between the outer and the inner layers [27], the area fraction of A/B in the outer layer is conserved. In the experimental situation [21], the amphiphilic molecules are preferentially absorbed from the surrounding solvent onto one of the two sides of the bilayer depending on whether the head of the amphiphile is cationic or anionic. The simple situation of our model mentioned above can be regarded as an idealization of such an experiment. On the other hand, the general case of bilayer membranes composed of a binary mixture (i.e., each two sides of the bilayer is composed of A and B amphiphiles) is rather complicated. Neglecting exchanges of amphiphiles between the inner and the outer layers, the area fraction of amphiphiles must be conserved in each two sides of bilayer. Safran *et al.* [13] and MacKintosh and Safran [14] have discussed such a general situation. Following their ideas, we can extend our model to include two order parameters $(\Phi_{\mathrm{in}} \pm \Phi_{\mathrm{out}})/2$ where Φ_{in} and Φ_{out} are relative compositions in the inner and the outer layers, respectively, where the coefficients A_i's of $\Phi = (\Phi_{\mathrm{in}} - \Phi_{\mathrm{out}})/2$ in equation (2.2) are shown to depend on $(\Phi_{\mathrm{in}} + \Phi_{\mathrm{out}})/2$.

Replacing the order parameter Φ with a *shifted* order parameter Ψ defined as

$$\Psi(u) \equiv \Phi(u) + \frac{A_3}{A_4} \qquad (2.6)$$

the free energy density $f(\Phi)$ can be written in term of Ψ where the third order term in Ψ vanishes

$$f(\Psi) = a_0 + a_1 \Psi + \frac{a_2}{2!} \Psi^2 + \frac{a_4}{4!} \Psi^4 \qquad (2.7)$$

The coefficients a_i ($i = 1, 2$ and 4) are related to the original A_i and μ. For systems close to a critical point of their phase separation, $a_2 = a(T - T_c^0)$ with $a > 0$, $a_4 > 0$ and T_c^0 is the bare critical temperature. This means that the homogeneous phase (where Ψ is single valued) becomes unstable for $T < T_c^0$. Using equation (2.6), the constraint (2.5) is rewritten as

$$\int \Psi(u) \sqrt{g} \, d^D u \equiv M = \begin{cases} \langle \Psi \rangle \, L & \text{in} \quad 2d \\ \langle \Psi \rangle \, S & \text{in} \quad 3d \end{cases} \qquad (2.8)$$

where M is the fixed total difference in the amount of A and B, and $\langle \Psi \rangle = \langle \Phi \rangle + A_3/A_4$. Taking the constraint (2.4) into account, the constant term a_0 turns out to give a constant contribution to the free energy and can be neglected. If one investigates the equilibrium state with a fixed M, the linear Ψ term in equation (2.7) can also be eliminated from $f(\Psi)$ due to a constant contribution of F. The linear term is only important for comparison of the system free energy with different M. However, in the following sections, we discuss equilibrium states with a fixed M, and drop the linear term in Ψ from equation (2.7).

The substitution of Φ by Ψ in the combined elastic energy terms, equations (2.1) and (2.3), gives rise to an *averaged* spontaneous curvature H_{sp}. We divide the total elastic energy into two terms : F_1 and F_3

$$F_1 = \frac{\kappa}{2} \int (H - H_{sp})^2 \sqrt{g} \, d^D u \qquad (2.9)$$

$$F_3 = \Lambda \int \Delta \Psi H \sqrt{g} \, d^D u \qquad (2.10)$$

$$H_{sp} \equiv \frac{\Lambda}{\kappa} \left(\frac{A_3}{A_4} - \langle \Psi \rangle \right) \qquad (2.11)$$

$$\Delta \Psi(u) \equiv \Psi(u) - \langle \Psi \rangle . \qquad (2.12)$$

For 2d vesicles, the following identity holds for simply-connected (circle like) shapes (see Appendix A)

$$\int H \sqrt{g} \, du = 2\pi . \qquad (2.13)$$

This identity implies that the averaged spontaneous curvature H_{sp} in F_1 [Eq. (2.9)] is irrelevant, while, F_3 expresses the *local* spontaneous curvature term, and is relevant for 2d vesicles. In 3d, no such identity as equation (2.13) exits. Hence the averaged spontaneous curvature H_{sp} as well as the local spontaneous curvature (the F_3 term) are relevant there. As is seen from equation (2.11), the averaged spontaneous curvature comes from *asymmetry* in the exchange of A and B ($A_3 \neq 0$) as well as the *asymmetry* in the A/B area fraction $\langle \Psi \rangle$.

Combining all contributions results in an expression for the total free energy $F = F_1 + F_2 + F_3 + PA$ ($F_1 + F_2 + F_3 + PV$ in 3d). As was explained above, the Ginzburg-Landau free energy functional F_2 has only even powers in terms of Ψ

$$F_2 = \int \left\{ \frac{b}{2} (\nabla \Psi)^2 + \frac{a_2}{2!} \Psi^2 + \frac{a_4}{4!} \Psi^4 \right\} \sqrt{g}\, d^D u \, . \tag{2.14}$$

In the following, we perform a linear stability analysis and investigate the phase diagram of equilibrium shape deformations of vesicles using the single-mode approximation (SMA) in two and three dimensions.

3. Vesicles in 2d space.

We now consider a one-dimensional closed contour, representing a vesicle embedded in 2d space (see Fig. 1). Such a 2d vesicle can also be regarded as a cross section of a cylindrical vesicle. The vesicle is composed of A and B species. It is convenient to choose the polar angle θ as the particular parametrization of the contour. This will replace the general parameter u of the preceding section (see Appendix A). We recall that two constraints of constant contour length and total amounts of A and B, equations (2.4) and (2.8), are imposed.

In what follows we limit our treatment to shallow temperature quenches close to the bare critical temperature T_c^0. In such situations, the deviation R of the vesicle radius $r(\theta)$ from a perfect circle is much smaller than the radius of the *reference* circle, r_0. Furthermore, the deviation of the order parameter $|\Delta \Psi|$ from its spatial average $\langle \Psi \rangle$ is much smaller than unity

$$r(\theta) = r_0 + R(\theta) \qquad |R(\theta)| \ll r_0 \tag{3.1}$$

$$\Psi(\theta) = \langle \Psi \rangle + \Delta \Psi(\theta) \qquad |\Delta \Psi| \ll 1 \, . \tag{3.2}$$

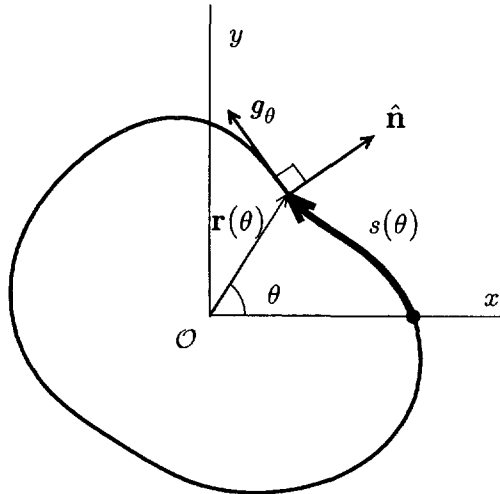In this case, the fixed total contour length of the 2d vesicle is taken as $L = 2\pi r_0$.

Fig. 1. — Parametrization of a 2d vesicle (contour) embedded in the xy-plane. Equivalently, this can be regarded as a cross section of a cylindrical vesicle extending to infinity along the z-axis. The polar angle between x-axis and the radius vector to a point on the contour is denoted by θ, while $s(\theta)$ denotes a contour length from $\theta = 0$. The tangential and normal unit vectors to the contour within the xy-plane are g_θ and $\hat{n}$, respectively.

3.1 LINEAR STABILITY ANALYSIS IN 2d. — In order to investigate the onset of instability of the vesicle shape, it is enough to retain terms up to second order in R and Ψ. Since all variables depending on θ are 2π-periodic functions, R and Ψ can be expressed as a Fourier series in θ (see Appendix D)

$$R(\theta) = c_0 + \sum_{n=1}^{\infty} [c_n \cos n\theta + s_n \sin n\theta] \tag{3.3}$$

$$\Psi(s(\theta)) = \Psi_0 + \sum_{n=1}^{\infty} \left[\Psi_{cn} \cos \frac{2\pi n}{L} s(\theta) + \Psi_{sn} \sin \frac{2\pi n}{L} s(\theta) \right] ; \quad 0 \leq s \leq L \tag{3.4}$$

where $s(\theta)$ is the contour length measured from the origin up to a point specified by θ (Fig. 1)

$$s(\theta) = \int_0^\theta (\dot{r}^2 + r^2)^{1/2} \, d\theta' \tag{3.5}$$

where $\dot{r}(\theta)$ denotes the derivative of $r(\theta)$ with respect to θ. To second order in c_n and s_n, the constant c_0 is determined from the constraint [Eq. (2.4) or $L = s(2\pi) = 2\pi r_0$].

$$c_0 = -\frac{1}{4 r_0} \sum_{n=1}^{\infty} n^2 (c_n^2 + s_n^2) . \tag{3.6}$$

Using the expression of the order parameter Ψ, [Eq. (3.4)], the constraint (2.8) is easily satisfied by taking Ψ_0 as

$$\Psi_0 = \langle \Psi \rangle \tag{3.7}$$

where $\langle \Psi \rangle \equiv M/2\pi r_0$. It is convenient to define $\pi\kappa/r_0$ as the unit of energy, as this is the bending energy for a perfect circular vesicle of radius r_0. Rescaling appropriately all quantities yields,

$$\left. \begin{array}{llll} \tilde{F} \equiv \dfrac{r_0}{\pi \kappa} F & \tilde{p} \equiv \dfrac{P r_0^3}{\kappa} & \tilde{c}_n \equiv \dfrac{c_n}{r_0} & \tilde{\Psi}_{cn} \equiv \dfrac{\Lambda r_0}{\kappa} \Psi_{cn} \\[4mm] \tilde{A} \equiv \dfrac{1}{\pi r_0^2} A & \tilde{a}_2 \equiv \dfrac{\kappa}{\Lambda^2} a_2 & \tilde{a}_4 \equiv \dfrac{\kappa^3}{\Lambda^4 r_0^2} a_4 & \tilde{b} \equiv \dfrac{b\kappa}{\Lambda^2 r_0^2} \end{array} \right\} \tag{3.8}$$

and $\tilde{s}_n$ and $\tilde{\Psi}_{sn}$ are defined in the same way as $\tilde{c}_n$ and $\tilde{\Psi}_{cn}$, respectively. To 2nd order in $\tilde{c}_n$, $\tilde{s}_n$, $\tilde{\Psi}_{cn}$ and $\tilde{\Psi}_{sn}$, each term of the rescaled free energy $\tilde{F}$ is expressed as :

$$\tilde{F}_1 = \frac{1}{2} \sum_{n=1}^{\infty} (n^2 - 1)^2 (\tilde{c}_n^2 + \tilde{s}_n^2) + \cdot \tag{3.9}$$

$$\tilde{F}_2 = \frac{1}{2} \sum_{n=1}^{\infty} \left(\tilde{b}n^2 + \tilde{a}_2 + \frac{\tilde{a}_4}{2} \langle \tilde{\Psi} \rangle^2 \right) (\tilde{\Psi}_{cn}^2 + \tilde{\Psi}_{sn}^2) + \cdot \tag{3.10}$$

$$\tilde{F}_3 = \sum_{n=1}^{\infty} (n^2 - 1)(\tilde{c}_n \tilde{\Psi}_{cn} + \tilde{s}_n \tilde{\Psi}_{sn}) + \cdot \tag{3.11}$$

$$\tilde{P}\tilde{A} = -\frac{\tilde{p}}{2} \sum_{n=1}^{\infty} (n^2 - 1) \tilde{c}_n^2 + \cdot \tag{3.12}$$

where $\langle \tilde{\Psi} \rangle \equiv \dfrac{\Lambda r_0}{\kappa} \langle \Psi \rangle$ and irrelevant constant terms are neglected.

Using equations (3.9-3.12), the total rescaled free energy $\tilde{F} = \tilde{F}_1 + \tilde{F}_2 + \tilde{F}_3 + \tilde{P}\tilde{A}$ is written as

$$\tilde{F} = \frac{1}{2} \sum_{n=1}^{\infty} \left[\tilde{D}_n(\tilde{c}_n^2 + \tilde{s}_n^2) + \tilde{E}_n(\tilde{\Psi}_{cn}^2 + \tilde{\Psi}_{sn}^2) + 2(n^2 - 1)(\tilde{c}_n \tilde{\Psi}_{cn} + \tilde{s}_n \tilde{\Psi}_{sn}) \right] + \cdot \qquad (3.13)$$

where the coefficients $\tilde{D}_n$ and $\tilde{E}_n$ are defined as

$$\tilde{D}_n \equiv (n^2 - 1)(n^2 - 1 - \tilde{p})$$
$$\tilde{E}_n \equiv \tilde{b}n^2 + \tilde{a}_2 + \frac{\tilde{a}_4}{2} \langle \tilde{\Psi} \rangle^2 \qquad (3.14)$$

A linear stability analysis can now be performed using equation (3.13). Two cases can be distinguished : (a) $\tilde{p} < \tilde{p}_c$; and, (b) $\tilde{p} \geqslant \tilde{p}_c$, where the threshold value $\tilde{p}_c$ for 2d vesicles is

$$\tilde{p}_c = 3 \qquad (3.15)$$

(a) $\tilde{p} < \tilde{p}_c = 3$. — In this case, $\tilde{D}_n > 0$ for all n modes beside the $n = 1$ mode. The circular shape is stable ($c_n = s_n = 0$) provided that the coupling term F_3 [the last term in Eq. (3.13)], vanishes. On the other hand, if there exists a coupling term ($\Lambda \neq 0$), an instability can take place. Linear stability analysis involves minimizing the free energy (3.13) with respect to $\tilde{c}_n$ and $\tilde{s}_n$

$$\left. \begin{array}{l} \tilde{c}_n = - \dfrac{1}{n^2 - 1 - \tilde{p}} \, \tilde{\Psi}_{cn} \\[2mm] \tilde{s}_n = - \dfrac{1}{n^2 - 1 - \tilde{p}} \, \tilde{\Psi}_{sn} \end{array} \right\} \quad \text{except for} \quad n = 1 . \qquad (3.16)$$

The shape of the $n = 1$ mode is a perfect circle if only terms up to the 2nd order in c_1 and s_1 are included in F_1. Higher than 2nd order terms result in small deviations from the circular shape. Therefore, for the 2nd order expansion employed here, the $n = 1$ mode describes a lateral phase separation while preserving the perfect circular shape. Eliminating $\tilde{c}_n$ and $\tilde{s}_n$ from $\tilde{F}$ by substituting equation (3.16) into equation (3.13), we get

$$\tilde{F} = \frac{1}{2} \sum_{n=1}^{\infty} \tilde{\Gamma}_n(\tilde{\Psi}_{cn}^2 + \tilde{\Psi}_{sn}^2) \qquad (3.17)$$

where

$$\tilde{\Gamma}_n \equiv \tilde{E}_n - \frac{n^2 - 1}{n^2 - 1 - \tilde{p}} \qquad (3.18)$$

From these expressions, an instability is found to occur for all modes n satisfying

$$\tilde{\Gamma}_n < 0 . \qquad (3.19)$$

An interesting limit is the one of infinitely large vesicles ($r_0 \to \infty$). Here, the vesicle resembles a fluctuating lamella. The discrete mode n has a continuum limit and is replaced by the wavenumber $q \equiv n/r_0$. Substituting this definition of q and the Laplace pressure

$P = -\sigma/r_0$, σ being the line tension, into equation (3.18), $\tilde{\Gamma}_n$ can be rewritten as

$$\tilde{\Gamma}_q = \hat{b}q^2 + \tilde{a}_2 - \frac{q^2}{q^2 + \sigma/\kappa} \tag{3.20}$$

where $\hat{b} = b\kappa/\Lambda^2$. This exactly coincides with previous results for membranes (lamella) fluctuating about a flat reference plane [9, 10, 12].

(b) $\tilde{p} \geqslant \tilde{p}_c = 3$. — In this case, $\tilde{D}_n \leqslant 0$ for some n modes. Therefore, the circular shape is unstable even *without* the coupling term F_3. All n modes satisfying the condition $\tilde{p} > n^2 - 1$ are unstable. Such an instability is induced by a pressure difference even for single-component vesicles [29]. Notice that in this case, the coupling term F_3 is not the only source of the instability for a mixed vesicle.

3.2 PHASE DIAGRAM IN 2d SPACE. — In order to study the phase transitions, we have to retain higher than 2nd-order terms in the free energy and look for minimum energy states among different modes. Here, we assume that the equilibrium state is described by a pure state with a single n mode. (Single mode approximation is abbreviated as SMA.) This is a reasonable approximation in the proximity of the critical point.

$$R(\theta) = c_0 + c_n \cos n\theta \tag{3.21}$$

$$\Psi(s(\theta)) = \Psi_0 + \Psi_n \cos \frac{2\pi n}{L} s(\theta) \tag{3.22}$$

where c_0 is determined so that the total contour length is conserved (see Appendix B). The constant term Ψ_0 is determined so as to satisfy the constraint (2.8) and results in equation (3.7). Using equations (3.21) and (3.22), the relevant terms up to 4th order in $\tilde{c}_n$ and $\tilde{\Psi}_n$ in the expansion of $\tilde{F}$ are

$$\tilde{F} \simeq \frac{1}{2}\left\{2(n^2-1)\tilde{c}_n\tilde{\Psi}_n + \tilde{D}_n\tilde{c}_n^2 + \tilde{E}_n\tilde{\Psi}_n^2 + \frac{1}{8}(n^2-1)(n^2-2)\tilde{c}_n^3\tilde{\Psi}_n\right.$$

$$\left. + \frac{1}{8}\left[n^6 + \frac{1}{2}(\tilde{p}+41)n^4 - (2\tilde{p}+23)n^2 + 6\right]\tilde{c}_n^4 + \frac{\tilde{a}_4}{16}\tilde{\Psi}_n^4\right\} + \cdot \tag{3.23}$$

where the first three terms in (3.23) coincide with (3.13). Note that the state specified by $(\tilde{c}_n, \tilde{\Psi}_n)$ can be mapped into the state $(-\tilde{c}_n, -\tilde{\Psi}_n)$ by a rotation.

In case (a) mentioned above where $\tilde{p} < \tilde{p}_c = 3$, the free energy $\tilde{F}$ [Eq. (3.23)] can be minimized with respect to $\tilde{c}_n$ without higher (3rd and 4th) order terms in $\tilde{c}_n$ [31]. The coefficient of the $\tilde{c}_n^2$ term, i.e., $\tilde{D}_n$, is positive for all n modes except for $n = 1$ corresponding to a translation of the circular vesicle as a whole. Then we obtain

$$\tilde{F} = \frac{1}{2}\left(\tilde{\Gamma}_n\tilde{\Psi}_n^2 + \frac{\tilde{a}_4}{16}\tilde{\Psi}_n^4\right) \tag{3.24}$$

and the minimum free energy is found to be :

$$\tilde{F} = \begin{cases} -\dfrac{2}{\tilde{a}_4}\tilde{\Gamma}_n^2 & \text{for} \quad \tilde{\Gamma}_n < 0 \\[2mm] 0 & \text{for} \quad \tilde{\Gamma}_n > 0 \,. \end{cases} \tag{3.25}$$

In case (b), $\tilde{p} \geqslant \tilde{p}_c = 3$, a circular shape is unstable due to the imposed pressure even without the coupling term [29]. Because $\tilde{D}_n \leqslant 0$ holds for several n modes, we must take into account terms up to 4th order in both $\tilde{c}_n$ and $\tilde{\Psi}_n$ to determine the lowest-energy. Numerical calculations are performed in order to find the free energy minima. However, when we discuss the relative stability between the $n = 1$ and $n \geqslant 2$ modes, we must retain terms up to 6th order in the total free energy since the coefficient of the 4th order term in $\tilde{c}_1$ is negative for $\tilde{p} > 3$ [this coefficient is $3(3 - \tilde{p})/2$ for $n = 1$ mode]. The coefficient of the 6th order term in $\tilde{c}_n$ is given by $[3\, n^8 + 22\, n^6 + 67\, n^4 - (2\, \tilde{p} + 56)\, n^2 + 10]/2^5$, and it reduces to $46 - 2\, \tilde{p}$ for the $n = 1$ mode. For simplicity, we have chosen to study the phase diagram in the region $-10 < \tilde{p} < 5$ where it was checked that the 6th order coefficient is always positive [32].

The validity of the single mode approximation (SMA) in the shallow quench limit can be justified only if the following two conditions are satisfied. First, the magnitude of the equilibrium value of the order parameter must be sufficiently small [see Eq. (3.2)]. Using equation (3.24), this condition reduces to the inequality

$$\left| \tilde{\Psi}_n \right| = \left(\frac{-8\, \tilde{\Gamma}_n}{\tilde{a}_4} \right)^{1/2} \ll 1 \quad \text{for} \quad \tilde{\Gamma}_n < 0 . \tag{3.26}$$

Furthermore, in the region $\tilde{p} \leqslant 0$, the inequality (3.26) reduces to

$$\frac{\tilde{a}_4}{8} \gg \left| 1 - \tilde{a}_2 \right| . \tag{3.27}$$

Note that condition (3.27) reduces to $\tilde{a}_4 \gg 1$ near T_c^0 ($\tilde{a}_2 \simeq 0$).

The second condition arises from the single mode approximation, where the order parameter is expressed by only a single sinusoidal mode. In this approximation, the A and B amphiphiles are weakly immiscible, i.e., the order parameter profile varies slowly at the domain boundary between A-rich and B-rich regions. The width of the domain boundary ξ is expressed as

$$\xi \simeq 2\, \pi r_0 \left(\frac{\tilde{b}}{1 - \tilde{a}_2} \right)^{1/2} \quad \text{for} \quad \tilde{a}_2 < 1 \tag{3.28}$$

and ξ must be the same order as a half of a wavelength of an equilibrium selected mode, n^*, as the equilibrium state

$$\xi \simeq \frac{1}{2} \cdot \frac{2\pi}{q^*} \tag{3.29}$$

where the wavenumber $q^* \equiv n^*/r_0$. The strong segregation limit, for $-\tilde{a}_2 \gg 1$, is the limit where the domain walls are sharp ($\xi \to 0$), and conditions (3.26) and (3.29) are violated. Hence, the single mode approximation is valid only close to the critical point. Near the bare critical temperature ($\tilde{a}_2 \simeq 0$), equation (3.29) provides the condition for the rescaled parameter $\tilde{b}$. This approximation is justified as long as $\tilde{b}^{-1/2} \simeq 2\, n^*$ As is mentioned below, the phase diagram is calculated in the rescaled parameter space, where both conditions, equations (3.26) and (3.29) are satisfied.

Phase diagrams in the rescaled parameter space $(\tilde{b}^{-1/2}, \tilde{p}, \tilde{a}_2)$ are obtained by numerical evaluations of the free energy, where all the terms up to 6th order in $\tilde{c}_n$ and $\tilde{\Psi}_n$ are taken into account (as was explained above). Shape deformations depend, in general, also on

$\langle \Psi \rangle$ as have been previously explored in the strong segregation limit [12]. For simplicity, we consider here only the $\langle \Psi \rangle = 0$ case. The phase diagram in the $(\tilde{b}^{-1/2}, \tilde{p})$ plane for the bare critical temperature, $T = T_c^0$ ($\tilde{a}_2 = 0$), is presented in figure 2a, and the phase diagram in the $(\tilde{b}^{-1/2}, \tilde{a}_2)$ plane for a rescaled pressure difference $\tilde{p} = -1$ is shown in figure 2b. For both phase diagrams, $\tilde{a}_4/8$ is taken as 100 satisfying condition (3.26). However, as long as this condition is satisfied, the precise value of $\tilde{a}_4$ will only have a minor effect on the phase diagram.
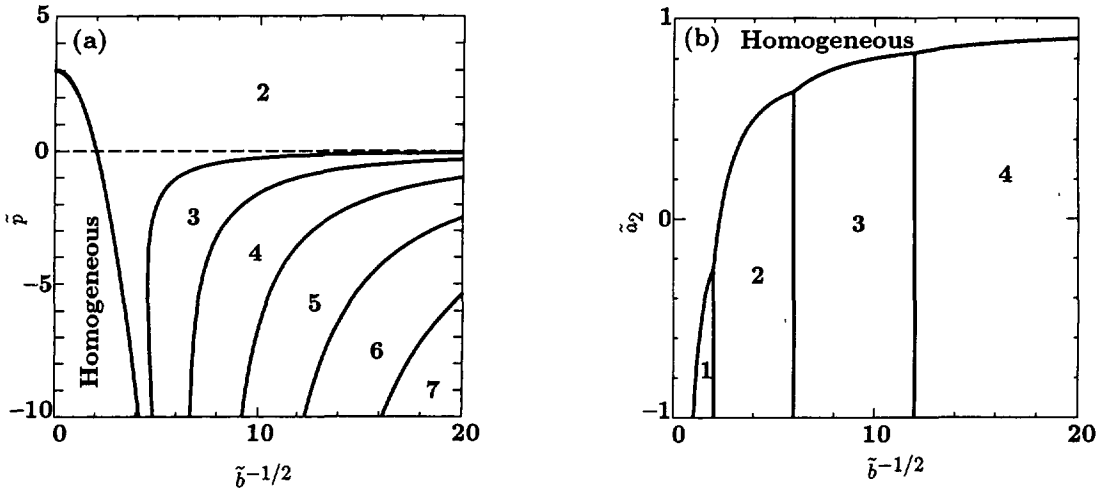

Fig. 2. — Phase diagrams for a 2d vesicle for : (a) the parameter plane $(\tilde{b}^{-1/2} \quad \tilde{p})$ with $\tilde{a}_2 = 0$, i.e., $(T = T_c^0)$; and (b) the parameter plane $(\tilde{b}^{-1/2} \quad \tilde{a}_2)$ with $\tilde{p} = -1$. The numbers in the figure stand for the most stable modes and « homogeneous » for the disordered homogeneous state with a perfect circular shape. In both cases (a) and (b), the spatial average of the order parameter is set as $\langle \Psi \rangle = 0$. The shifted critical temperature is given by the line between « homogeneous » and selected n-mode states. This line is a line of second-order phase transition, whereas all other lines are of first order. For $\tilde{p} \geqslant \tilde{p}_c = 3$, the mechanism of the mode selection is same as that of single-component vesicles [29], and where the $n = 2$ mode is always selected.

The lines denoting phase boundaries between regions with different stable modes, are obtained by *numerical* evaluation of the free-energy minima, and include terms up 6th order. We remark that almost identical results can also be obtained by evaluating *analytically* the free energy minima in equation (3.25) for $\tilde{p} < \tilde{p}_c = 3$. On the other hand, for $\tilde{p} > \tilde{p}_c = 3$, numerical evaluations using all terms up to the 6th order are necessary because lower order terms have negative coefficients.

As can be seen from the phase diagrams (Fig. 2), equilibrium shape deformations with non-trivial $n > 1$ modes are found. The $n = 1$ mode seen in figure 2b has a phase separation with only two domains while keeping an « almost » circular shape. One also sees from figure 2b that the critical temperature given by the line separating « homogeneous » and the other selected phases ($n = 1$, 2, 3,), is shifted from the bare critical temperature T_c^0 ($\tilde{a}_2 = 0$) and depends on the effective coupling coefficient $\tilde{b}^{-1/2}$ This line is (within our mean-field treatment) a line of second-order phase transitions, whereas all the other transition lines

are of first order with a jump in the order parameter. The shifted critical temperature T_c approaches $T_c^0 + \Lambda^2/a\kappa$ (i.e., $\tilde{a}_2 = 1$), as $\tilde{b}^{-1/2}$ becomes larger [9, 11]. On the other hand, the $\tilde{b}^{-1/2}$ dependence of T_c for smaller $\tilde{b}^{-1/2}$ comes from the finite size effect of the vesicle.

In figure 2a, the $n = 2$ mode is selected in the region $\tilde{p} \geqslant 3$ due to the energy gain coming from the pressure difference term just as for single-component 2d vesicles [29]. On the other hand, for $\tilde{p} < 3$, the coupling term F_3 and the domain boundary energy play an important role in determining the equilibrium state. While F_3 prefers higher modes, the domain boundary energy, proportional to the gradient term in F_2, prefers smaller domain boundaries, or equivalently smaller mode numbers. The most stable mode is determined by the competition between F_3, the coupling term, and the gradient term in F_2. Therefore, higher modes are selected as the effective coupling coefficient $\tilde{b}^{-1/2}$ becomes larger.

4. Vesicles in 3d space.

Now we consider a two-component vesicle embedded in 3d space. This system is characterized by the total free energy F and two constraints (fixed total area and fixed amounts of each of the A and B species) as described in section 2. The vesicles is represented by a closed surface with the spherical topology. Using spherical coordinates (r, θ, φ), the position vector $\mathbf{r}$ from the origin to a point on the vesicle is expressed as $\mathbf{r} = r(\theta, \varphi) \mathbf{e}_r$ where $\mathbf{e}_r$ is a unit vector, r is the radius and θ and φ are the polar and azimuthal angles, respectively. More technical details are explained in Appendix A.

As for 2d vesicles, we consider here only a shallow temperature quench in the vicinity of the critical point, where the vesicle is nearly a perfect sphere, and the A and B amphiphiles are weakly segregated. Therefore, the deviation $R(\theta, \varphi)$ from a perfect sphere of a radius r_0 and the deviation $\Delta\Psi(\theta, \varphi)$ of the order parameter from its average value $\langle\Psi\rangle$ are small.

$$\begin{aligned} r(\theta, \varphi) &= r_0 + R(\theta, \varphi) & |R(\theta, \varphi)| &\ll r_0 \\ \Psi(\theta, \varphi) &= \langle\Psi\rangle + \Delta\Psi(\theta, \varphi) & |\Delta\Psi(\theta, \varphi)| &\ll 1 . \end{aligned} \tag{4.1}$$

The fixed total area of the vesicle is taken as $S = 4\pi r_0^2$.

4.1 LINEAR STABILITY ANALYSIS IN 3d. — As was shown in section 3, it is enough to take into account terms up to second order in R and $\Delta\Psi$ in order to investigate the onset of the instability. Since the vesicle has a closed form with a spherical topology, it is convenient to expand $R(\theta, \varphi)$ and $\Psi(\theta, \varphi)$ in spherical harmonics [33]

$$\left.\begin{aligned} R(\theta, \varphi) &\doteq C_0 + \sum_{\ell=1}^{\infty} \sum_{m=-\ell}^{\ell} C_{\ell m} Y_{\ell m}(\theta, \varphi) \\ \Psi(\theta, \varphi) &= \Psi_0 + \sum_{\ell=1}^{\infty} \sum_{m=-\ell}^{\ell} \Psi_{\ell m} Y_{\ell m}(\theta, \varphi) \end{aligned}\right\} \tag{4.2}$$

where the spherical harmonics are $Y_{\ell m} \equiv N_{\ell m} P_\ell^m(\cos\theta) e^{im\varphi}$, $P_\ell^m(\cos\theta)$ are the associated Legendre polynomials and the normalization constant $N_{\ell m} \equiv \left[\dfrac{2\ell+1}{4\pi} \dfrac{(\ell - |m|)!}{(\ell + |m|)!} \right]^{\frac{1}{2}}$ While the expansion coefficients $C_{\ell m}$ and $\Psi_{\ell m}$ are complex numbers, the relations $C_{\ell m}^* = C_{\ell, -m}$ and $\Psi_{\ell m}^* = \Psi_{\ell, -m}$ guarantee that R and Ψ are real functions. The $\ell = 0$ contribution, C_0, is determined from the condition that the total area of the vesicle is conserved [Eq. (2.4)]. Using the expansion in equation (4.2), C_0 can be expressed by the amplitudes of other

$\ell \geqslant 1$ modes $(C_{\ell m})$ keeping only terms up to 2nd order.

$$C_0 = -\frac{1}{16\pi r_0} \sum_{\ell=1}^{\infty} \sum_{m=-\ell}^{\ell} \left(\ell(\ell+1) + 2 \right) |C_{\ell m}|^2 \qquad (4.3)$$

The second constraint of fixed total amount of amphiphiles [Eq. (2.8)] gives the following relation

$$\Psi_0 = \langle \Psi \rangle - \frac{1}{2\pi r_0} \sum_{\ell=1}^{\infty} \sum_{m=-\ell}^{\ell} C_{\ell m} \Psi_{\ell,-m} \qquad (4.4)$$

where $\langle \Psi \rangle \equiv M/4\pi r_0^2$ and the second term includes corrections due to shape deformation. Using expansion (4.2) and the constraints (4.3) and (4.4), the total free energy up to 2nd order in $C_{\ell m}$ and $\Psi_{\ell m}$ can be written as

$$\tilde{F} = \frac{1}{16\pi} \sum_{\ell=1}^{\infty} \sum_{m=-\ell}^{\ell} \left[\left(\ell(\ell+1) - 2 \right)\left(\ell(\ell+1) - \tilde{H}_{\rm sp} - \tilde{p} \right) |\tilde{C}_{\ell m}|^2 \right.$$
$$\left. + \left(\tilde{b}\ell(\ell+1) + \tilde{a}_2 + \frac{\tilde{a}_4}{2} \langle \tilde{\Psi} \rangle^2 \right) |\tilde{\Psi}_{\ell m}|^2 + 2(\ell(\ell+1) - 2) \tilde{C}_{\ell m} \tilde{\Psi}_{\ell m}^* \right] \qquad (4.5)$$

where $\langle \tilde{\Psi} \rangle \equiv \dfrac{\Lambda r_0}{\kappa} \langle \Psi \rangle$. The definitions of the rescaled (tilde) parameters are the same as those for the 2d case [see Eq. (3.8)], except for the rescaled pressure and spontaneous curvature, which are defined in the present 3d case as $\tilde{p} \equiv P r_0^3/2\kappa$ and $\tilde{H}_{\rm sp} \equiv H_{\rm sp} r_0$, respectively. We take $8\pi\kappa$ as the energy unit since it is the elastic bending energy of a perfect 3d spherical vesicle without spontaneous curvature. In expression (4.5), our results of the elastic energy $\tilde{F}_1$ and the osmotic pressure term $\tilde{P}\tilde{V}$ [first line of Eq. (4.5)] are identical to previous results for single-component vesicles [34, 35]. The expression of the free energy for 3d vesicle [Eq. (4.5)] has almost the same features as that for 2d vesicle [Eq. (3.13)], except for the appearance of the spontaneous curvature. It should be noted that the states with different values of m but with the same ℓ value are degenerate. Two cases can be distinguished (similar to the 2d case), and are discussed separately : (a) $\tilde{p} < \tilde{p}_{\rm c}$ and (b) $\tilde{p} \geqslant \tilde{p}_{\rm c}$, where the threshold in pressure difference is defined as

$$\tilde{p}_{\rm c} = 6 - \tilde{H}_{\rm sp} . \qquad (4.6)$$

(a) $\tilde{p} < \tilde{p}_{\rm c}$. — In this case the spherical vesicle is stable if the coupling term $\tilde{F}_3$ is absent. However, in the presence of the coupling, the spherical vesicle can become unstable. Investigations of such an instability can be performed by minimizing the free energy (4.5) with respect to $\tilde{C}_{\ell m}(\tilde{C}_{\ell m}^*)$

$$\tilde{C}_{\ell m} = -\frac{1}{\ell(\ell+1) - \tilde{H}_{\rm sp} - \tilde{p}} \tilde{\Psi}_{\ell m} \qquad (\ell \neq 1) . \qquad (4.7)$$

Eliminating $\tilde{C}_{\ell m}$ from the free energy using equation (4.7), the minimum free energy is expressed as

$$\tilde{F} = \frac{1}{16\pi} \sum_{\ell=1}^{\infty} \sum_{m=-\ell}^{\ell} \tilde{\Gamma}_\ell |\tilde{\Psi}_{\ell m}|^2 \qquad (4.8)$$

where $\tilde{\Gamma}_\ell$ is defined as

$$\tilde{\Gamma}_\ell \equiv \tilde{b}\ell(\ell+1) + \tilde{a}_2 + \frac{\tilde{a}_4}{2}\langle\tilde{\Psi}\rangle^2 - \frac{\ell(\ell+1)-2}{\ell(\ell+1)-\tilde{H}_{sp}-\tilde{p}} \qquad (4.9)$$

where $\ell = 1$ mode is included in equation (4.9). Therefore, the instability occurs for the modes satisfying the inequality $\tilde{\Gamma}_\ell < 0$.

In the limit of an infinitely large vesicle $(r_0 \to \infty)$, the discrete ℓ mode reduces to a continuous wavenumber q $(\ell = r_0 q)$. The same expression as for an almost flat fluid membrane is obtained [see also Eq. (3.20) for 2d vesicles].

(b) $\tilde{p} \geqslant \tilde{p}_c$. — In this case. the circular vesicle is unstable even without the coupling term. The inequality $\tilde{p} \geqslant \tilde{p}_c$ is the same as the criterion for the onset of instability in single-component 3d vesicles [2-4, 34, 35] of the $\ell = 2$ mode. More generally, the onset of instability of any $\ell \geqslant 2$ mode is given by the threshold pressure $\tilde{p}_c(\ell)$

$$\tilde{p} > \tilde{p}_c(\ell) \equiv \ell(\ell+1) - \tilde{H}_{sp}. \qquad (4.10)$$

4.2 PHASE DIAGRAM IN 3d SPACE. — We now consider the equilibrium phase diagram of 3d vesicles for shallow temperature quenches, where the deviations of the order parameter from its average value and that of the vesicle shape from a perfect sphere are small. For simplicity, we restrict our treatments to axial symmetric shape deformations and axial symmetric order parameters (having only $m = 0$ modes). As for 2d vesicles, we assume that the equilibrium state is characterized by a single mode (the single mode approximation SMA)

$$R(\theta) = C_0 + C_\ell P_\ell(\cos\theta) \qquad \ell \neq 0 \qquad (4.11)$$

where $C_\ell \equiv C_{\ell 0} N_{\ell 0}$. The constraint (2.4) on the total area of the vesicle surface determines C_0

$$C_0 = -\frac{1}{4r_0} \cdot \frac{\ell(\ell+1)+2}{2\ell+1}(C_\ell)^2 - \sum_{n=3}^{6} \frac{\alpha_n}{r_0^{n-1}}(C_\ell)^n + \cdot \qquad (4.12)$$

Detailed expressions of α_n up to 6th order are given in Appendix C. Expansion up to 6th order in C_ℓ is needed in order to evaluate free energy minima as is explained in Appendix C. Using equation (4.12), the sum of the bending energy and the osmotic pressure energy of the vesicle $(\tilde{F}_s \equiv \tilde{F}_1 + \tilde{P}\tilde{V})$ is found to be :

$$\tilde{F}_s = \frac{1}{4}\frac{1}{2\ell+1}\left(\ell(\ell+1)-2\right)\left(\ell(\ell+1)-\tilde{H}_{sp}-\tilde{p}\right)(\tilde{C}_\ell)^2$$
$$-\frac{1}{8}\left[\left(1+\frac{\tilde{H}_{sp}}{2}\right)\left(\ell^2(\ell+1)^2-2\ell(\ell+1)\right)-\frac{4}{3}\tilde{p}\right]I_3^{(0)}(\ell)(\tilde{C}_\ell)^3$$
$$+\sum_{n=4}^{6} W^{(n)}(\ell,\tilde{H}_{sp},\tilde{p})(\tilde{C}_\ell)^n + \cdot \qquad (4.13)$$

where $\tilde{C}_\ell \equiv C_\ell/r_0$ and $I_3^{(0)}(\ell)$ is defined as

$$I_3^{(0)}(\ell) \equiv \int_{-1}^{1}[P_\ell(w)]^3\,dw = \frac{2}{2\ell+1}\langle\ell,\ell;0,0|\ell,0\rangle^2 \geqslant 0 \qquad (4.14)$$

where $\langle \ell_1, \ell_2 ; m_1, m_2 | \ell_3, m_3 \rangle$ are the *Clebsch-Gordan* coefficients [36]. Detailed expressions of $W^{(n)}$ up to 6th order are given in Appendix C. The integral $I_3^{(0)}(\ell)$ is non-vanishing only for even ℓ. This implies that shape deformations specified by $\tilde{C}_\ell$ and $- \tilde{C}_\ell$ are different for even ℓ (i.e., a *prolate* shape for $\tilde{C}_\ell > 0$ and an *oblate* one for $\tilde{C}_\ell < 0$). For odd ℓ, these two shape deformations are identical but spatially inverted. Therefore, the bending energy term $\tilde{F}_1$ and pressure term $\tilde{P}\tilde{V}$ do not include odd power terms in $\tilde{C}_\ell$ with odd ℓ.

4.2.1 *Single-component vesicles.* — We look first at shape deformations of a single-component vesicle using the free energy $\tilde{F}_s = \tilde{F}_1 + \tilde{P}\tilde{V}$. As was mentioned in case (b) above, the ℓ-mode state becomes unstable at a pressure $\tilde{p} = \tilde{p}_c(\ell)$. For even ℓ, the two states with opposite signs but same amplitude of $\tilde{C}_\ell$ are degenerate only when terms up to 2nd order in $\tilde{C}_\ell$ are taken into account. However, this degeneracy is lifted when 3rd order term in $\tilde{C}_\ell$ is considered in the expansion of $\tilde{F}_s$. Depending on the sign of the 3rd order term, one of the two states is preferred. The criterion of the selection between the two states at the threshold pressure $\tilde{p} = \tilde{p}_c(\ell)$ is as follows. The prolate shape with a positive value of $\tilde{C}_\ell$ is selected for $\tilde{H}_{sp}$ greater than a critical spontaneous curvature $\tilde{H}_{sp}^c(\ell)$

$$\tilde{H}_{sp} > \tilde{H}_{sp}^c(\ell) \equiv - \frac{2\,\ell(\ell+1)(3\,\ell(\ell+1)-10)}{3\,\ell^2(\ell+1)^2 - 6\,\ell(\ell+1) + 8} \qquad \text{for even } \ell \qquad (4.15)$$

Otherwise, the oblate shape with a negative value of $\tilde{C}_\ell$ is selected. It should be noted [4, 33, 35] that if one inserts $\ell = 2$ in criterion (4.15), a prolate-ellipsoid shape $(\tilde{C}_2 > 0)$ is selected for $\tilde{H}_{sp} > -1.2$. Otherwise, an oblate-ellipsoid one $(\tilde{C}_2 < 0)$ is selected [37]. This can be seen in figure 3, where the dashed lines are irrelevant for single-component vesicles.

We also calculated free energy branches for different modes using equation (4.13). The coefficient of the highest-order term in $\tilde{C}_\ell$ considered here must be positive to evaluate the

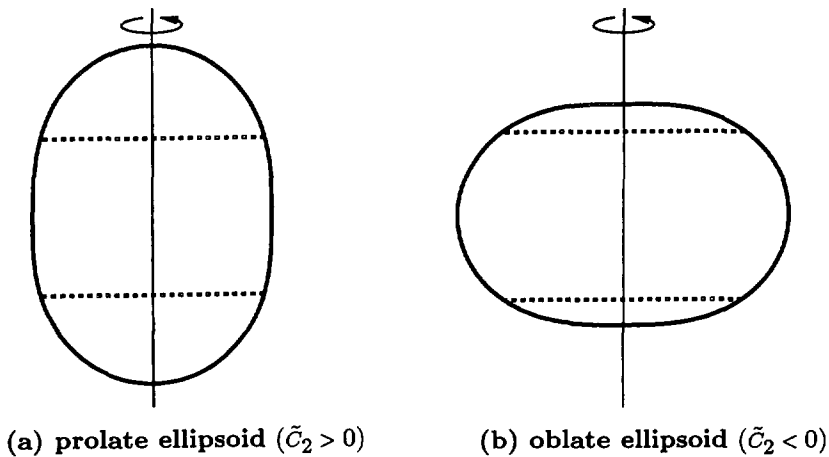**(a) prolate ellipsoid $(\tilde{C}_2 > 0)$**   **(b) oblate ellipsoid $(\tilde{C}_2 < 0)$**

Fig. 3. — Schematic views of vesicle shape deformations with an $\ell = 2$ mode for (a) $\tilde{C}_2 > 0$ (a prolate ellipsoid) and (b) $\tilde{C}_2 < 0$ (an oblate ellipsoid). These have the same amplitude of $\tilde{C}_2$. The dashed lines denote phase boundaries ($\Psi = 0$ lines) between A-rich and B-rich regions.

energy minima. The coefficient of the fourth order term $(\tilde{C}_\ell)^4$ in $\tilde{F}_1$ is negative for $\ell \geq 3$ (see Appendix C). Hence, here and in the following, we take into account terms up to 6th order, where the coefficient of $(\tilde{C}_\ell)^6$ is positive for any ℓ. In figure 4, free energy branches of the $\ell = 2$ mode are shown. In figure 4a, the free energy $\tilde{F}_s$ is shown as a function of the rescaled pressure for $\tilde{H}_{sp} = 0$. The metastable branch of a prolate-ellipsoid shape emerges at pressure $\tilde{p}_2 \simeq 5.938$. A first-order phase transition from a spherical shape to a prolate-ellipsoid shape takes place at $\tilde{p} = \tilde{p}_1 \simeq 5.945$ [38]. For $\tilde{p} > \tilde{p}_1$ the prolate-ellipsoid shape is selected, while an oblate-ellipsoid shape is a metastable state for $\tilde{p} > \tilde{p}_c = 6$. A spherical shape is stable for $\tilde{p} < \tilde{p}_1$, metastable for $\tilde{p}_1 < \tilde{p} < \tilde{p}_c$ and unstable for $\tilde{p} > \tilde{p}_c$. In addition, free energy branches for non-zero spontaneous curvature are shown in figure 4b for a particular value of $\tilde{H}_{sp} = -2$. In contrast to figure 4a, an oblate-ellipsoid shape emerges as a metastable state at $\tilde{p} = \tilde{p}_2 \simeq 7.970$, and is selected as the lowest energy state for $\tilde{p} > \tilde{p}_1 \simeq 7.973$. On the other hand, a prolate-ellipsoid shape is metastable for $\tilde{p} > \tilde{p}_c = 8$, as can be seen from equation (4.15). A spherical shape is stable for $\tilde{p} < \tilde{p}_1$, metastable for $\tilde{p}_1 < \tilde{p} < \tilde{p}_c$.

4.2.2 Two-component vesicles. — Now we consider the Ginzburg-Landau free energy $\tilde{F}_2$. The domain boundary energy between an A-rich and a B-rich regions is described by the gradient term in $\tilde{F}_2$. When the deformed shape and the order parameter (see Appendix D) are
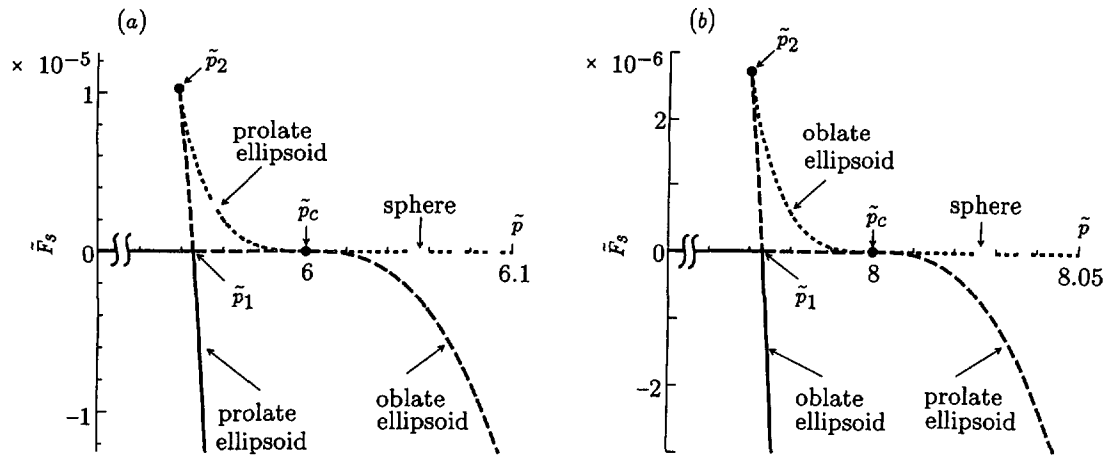

Fig. 4. — Free energy $\tilde{F}_s = \tilde{F}_1 + \tilde{P}\tilde{V}$ is plotted *versus* the rescaled pressure difference $\tilde{p}$ for two typical cases : (a) $\tilde{H}_{sp} = 0$; and (b) $\tilde{H}_{sp} = -2$. Free energy branches of three kinds of shapes are shown : a prolate-ellipsoid ($\tilde{C}_2 > 0$), an oblate-ellipsoid ($\tilde{C}_2 < 0$), and a sphere ($\tilde{C}_2 = 0$). The solid lines represent states of the minimal free energy. The dashed lines stand for metastable states, and the dotted ones for unstable states corresponding to maxima of $\tilde{F}_s$. The $\tilde{p}$-axis itself is the branch of a perfect sphere. (a) For $\tilde{H}_{sp} = 0$, the metastable prolate-ellipsoid branch emerges at $\tilde{p} = \tilde{p}_2 \simeq 5.938$. A first-order phase transition from a perfect spherical shape to a prolate-ellipsoid shape occurs at $\tilde{p} = \tilde{p}_1 \simeq 5.945$. The oblate-ellipsoid one is metastable for $\tilde{p} > \tilde{p}_c = 6$. (b) For $\tilde{H}_{sp} = -2$, the metastable oblate-ellipsoid branch emerges at $\tilde{p} = \tilde{p}_2 \simeq 7.970$, and becomes stable for $\tilde{p} > \tilde{p}_1 \simeq 7.973$. The prolate-ellipsoid branch is metastable for $\tilde{p} = \tilde{p}_c > 8$. In both cases of (a) and (b), a spherical shape is stable for $\tilde{p} < \tilde{p}_1$, metastable for $\tilde{p}_1 < \tilde{p} < \tilde{p}_c$ and unstable for $\tilde{p} > \tilde{p}_c$.

taken to depend only on a single ℓ mode, the gradient term in $\tilde{F}_2$ can be calculated

$$\int \sqrt{g}\,(\nabla \Psi(\theta))^2\,d\theta\,d\varphi$$

$$= 4\pi\,\Psi_\ell^2\left[\frac{\ell(\ell+1)}{2\ell+1} - \ell(\ell+1)\,I_3^{(0)}(\ell)\,\tilde{C}_\ell + G_4(\ell)(\tilde{C}_\ell)^2 + \cdot\quad\right]. \quad (4.16)$$

The detailed calculation of $G_4(\ell)$ is shown in Appendix D. Here we consider the influence of the domain boundary energy on the equilibrium state. For 2d vesicles, the domain boundary energy is only proportional to n^2 where n is the mode number (number of domain boundaries) [see Eq. (3.13)]. On the other hand, for 3d vesicles, the domain boundary energy depends on the shape deformation [the second and third terms of Eq. (4.16)] as well as on the number of domain boundaries (the first term). Fewer domain boundaries (small ℓ mode) are preferred in the same way as for 2d vesicles.

Furthermore, the domain boundary energy influences the shape deformations. For even ℓ, the domain boundary energy, [Eq. (4.16)] implies that the prolate shape ($\tilde{C}_\ell > 0$) is preferred over the oblate shape ($\tilde{C}_\ell < 0$), due to the second term in the r.h.s. of equation (4.16). This is because the shape with $C_\ell > 0$ has smaller domain boundary regions than that with $\tilde{C}_\ell < 0$ (see Fig. 3 as an example of a shape deformation with $\ell = 2$, where the dashed lines stand for domain boundaries defined by $\Psi = 0$ lines between A-rich and B-rich regions). For odd $\ell > 1$, shape deformations ($\tilde{C}_\ell \neq 0$) are preferred, because odd powers in $\tilde{C}_\ell$ in equation (4.16) vanish and $G_4(\ell)$ is always negative for $\ell \geq 3$. Namely, the domain boundary energy induces shape deformations in order to reduce domain boundary regions [12, 16, 17] for both even and odd modes. Moreover, when the contribution of domain boundary energy to the total free energy is sufficiently large, such intramembrane domains may induce budding of the membrane in agreement with previous results [16, 17].

Other terms in $\tilde{F}_2$ are easily calculated using equations (D.7-D.9) and the relevant terms in the free energy $\tilde{F}_2$ are expressed as

$$\tilde{F}_2 = \left[\frac{1}{4(2\ell+1)}\left(\tilde{a}_2 + \frac{\tilde{a}_4}{2}\langle\tilde{\Psi}\rangle^2\right) + \frac{\tilde{b}}{4}\left(\frac{\ell(\ell+1)}{2\ell+1}\right.\right.$$

$$\left.\left. - \ell(\ell+1)\,I_3^{(0)}(\ell)\,\tilde{C}_\ell + G_4(\ell)(\tilde{C}_\ell)^2 + \cdot\quad\right)\right]\tilde{\Psi}_\ell^2 + \frac{\tilde{a}_4}{24}\langle\tilde{\Psi}\rangle\,I_3^{(0)}(\ell)\,\tilde{\Psi}_\ell^3 + \frac{\tilde{a}_4}{96}I_4^{(0)}(\ell)\,\tilde{\Psi}_\ell^4$$

$$(4.17)$$

where $I_4^{(0)}(\ell)$ is defined and calculated in Appendix C, and $\langle\tilde{\Psi}\rangle$ is the rescaled spatial average of Ψ.

The coupling term $\tilde{F}_3$ is also calculated using the single mode approximation and is found to be

$$\tilde{F}_3 = \frac{1}{2}\frac{\ell(\ell+1)-2}{2\ell+1}\tilde{C}_\ell\,\tilde{\Psi}_\ell - \frac{1}{4}\ell(\ell+1)\,I_3^{(0)}(\ell)(\tilde{C}_\ell)^2\,\tilde{\Psi}_\ell + S_4(\ell)(\tilde{C}_\ell)^3\,\tilde{\Psi}_\ell + \cdot \quad (4.18)$$

A detailed derivation of equation (4.18) and explicit expressions of S_4 are shown in Appendix D.

We now consider the influence of the coupling term on the mode selection of the equilibrium state. Higher mode states with $\tilde{C}_\ell\,\tilde{\Psi}_\ell < 0$ are preferred as is seen from the first term in

equation (4.18). For odd ℓ, we note that the state with $\tilde{C}_\ell < 0$ ($\tilde{\Psi}_\ell > 0$) and the state with $\tilde{C}_\ell > 0$ ($\tilde{\Psi}_\ell < 0$) are identical but spatially inverted. For even ℓ, the state with $\tilde{C}_\ell < 0$ and $\tilde{\Psi}_\ell > 0$ is preferred due to the 3rd order term [$\sim (\tilde{C}_\ell)^2 \tilde{\Psi}_\ell$]. As an example, for the $\ell = 2$ mode (see Fig. 3), an oblate-ellipsoid shape ($\tilde{C}_2 < 0$ and $\tilde{\Psi}_2 > 0$) is preferred over a prolate-ellipsoid shape ($\tilde{C}_2 > 0$ and $\tilde{\Psi}_2 < 0$). We remark that the effect of the coupling term $\tilde{F}_3$ is contrary to and in competition with that of the domain boundary [Eq. (4.16)], which prefers shapes with $\tilde{C}_\ell > 0$ in order to reduce the domain boundary energy.

In order to obtain phase diagrams, we evaluated numerically the minima of the total free energy using equations (4.13), (4.17) and (4.18). It is enough to retain terms up to the fourth order in $\tilde{C}_\ell$ and $\tilde{\Psi}_\ell$ to see the influence of $\tilde{F}_2$ and $\tilde{F}_3$ on the equilibrium state selection. While for $\tilde{F}_s = \tilde{F}_1 + \tilde{P}\tilde{V}$, we had to retain terms up to the 6th order since the coefficient of the highest order terms in $\tilde{C}_\ell$ taken into account must be always positive. The phase diagram is calculated in the rescaled parameter space ($\tilde{b}^{-1/2}$, $\tilde{p}$, $\tilde{a}_2$, $\tilde{H}_{sp}$).

Since we used the single mode approximation in the shallow temperature quench, we have to impose validity limits on the parameters $\tilde{a}_4$ and $\tilde{b}$ as was done for 2d vesicles [see Eqs. (3.26) and (3.29)]. As long as equation (3.26) is satisfied, the precise value of the parameter $\tilde{a}_4$ is not of importance and was arbitrary chosen to be 2 000. The area fraction $\langle \tilde{\Psi} \rangle$ is a relevant parameter. Such a $\langle \tilde{\Psi} \rangle$ dependence of shape deformations for 3d two-component vesicles (where the coupling energy F_3 is not taken into account) was explored by Jülicher and Lipowsky [17] for domain-induced budding of axisymmetric 3d vesicles. Here, for simplicity, we choose $\langle \tilde{\Psi} \rangle = 0$. In figures 5 and 6, we show the calculated phase diagrams for $\tilde{H}_{sp} = 0$ and for $\tilde{H}_{sp} = -2$, respectively. In these figures, the ($\pm$) superscript stands for the sign of $\tilde{C}_\ell$ in the selected state. Other definitions are the same as those of figure 2. One of our main findings apparent from these figures is a selection of equilibrium shape deformations with non-trivial $\ell > 1$ modes. The $\ell = 1$ mode seen in figures 5b and 6b gives rise to the phase separation while keeping an « almost » spherical shape. (The spherical shape is slightly distorted if higher order terms are included in the expansion.)

The mechanism of such a mode selection is described as follows. As is seen in figures 5a and 6a, the mode with $\ell = 2$ is selected for $\tilde{p} \geq \tilde{p}_c$ due to the pressure difference in the same way as a single-component vesicle becomes unstable. The shapes with opposite signs of $\tilde{C}_2$ are different than the 2d case. A prolate-ellipsoid shape ($\tilde{C}_2 > 0$) is selected for $\tilde{H}_{sp} = 0$, while an oblate-ellipsoid one ($\tilde{C}_2 < 0$) is selected for $\tilde{H}_{sp} = -2$ according to the criterion (4.15) which gives a critical value of $\tilde{H}_{sp}^c(\ell = 2) = -1.2$. For $\tilde{p} < \tilde{p}_c$, the mode selection is determined by the competition between $\tilde{F}_2$ and $\tilde{F}_3$. A state with fewer domain boundaries is preferred by $\tilde{F}_2$ [Eq. (4.17)] while $\tilde{F}_3$ prefers high ℓ-mode states due to the first term in equation (4.18). Therefore, higher modes are selected as the effective coupling constant $\tilde{b}^{-1/2}$ becomes larger.

Moreover, for even ℓ, a selection between the states with opposite signs of $\tilde{C}_\ell$ is shown in figures 5 and 6. Such a selection is determined by the energy difference coming from second and third terms in equations (4.16) and (4.18). One can see that $\tilde{F}_2$ prefers shape deformations with $\tilde{C}_\ell > 0$ in order to reduce the domain boundary region due to the second term in equation (4.16). On the other hand, $\tilde{F}_3$ prefers a $\tilde{C}_\ell < 0$ state due to the second term in equation (4.18).
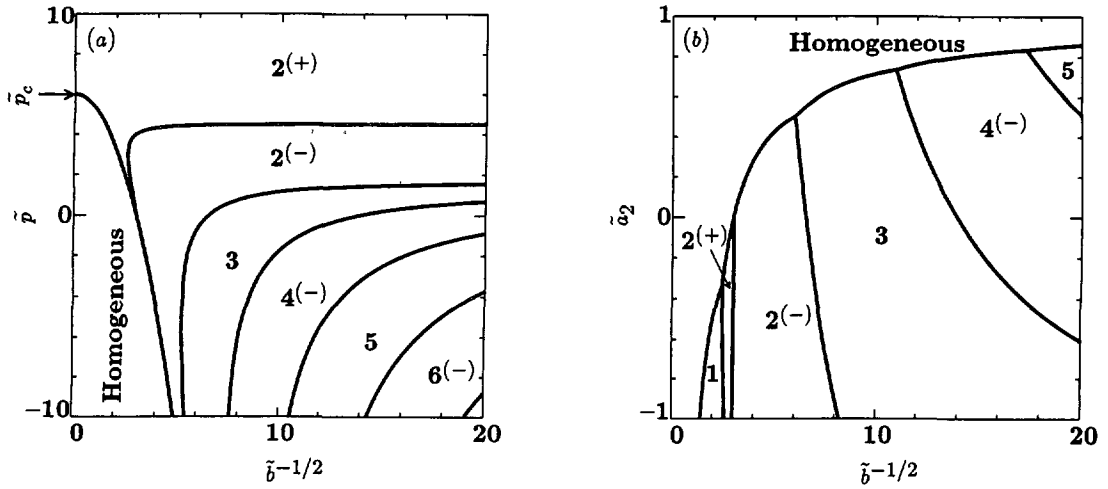
Fig. 5. — Phase diagrams of 3d vesicles with no spontaneous curvature $(\tilde{H}_{sp} = 0)$, are shown (a) in the parameter plane $(\tilde{p}, \tilde{b}^{-1/2})$ with $\tilde{a}_2 = 0$, i.e. $(T = T_c^0)$; and (b) $(\tilde{a}_2(T), \tilde{b}^{-1/2})$ with $\tilde{p} = 0$. The numbers and the ($\pm$) superscript stand for the most stable modes and the sign of $\tilde{C}_\ell$, respectively. « Homogeneous » means the disordered state with a perfect spherical shape. For $\tilde{p} \geqslant \tilde{p}_c = 6$, the mode selection is determined by the pressure difference in the same way as single-component vesicles [2-4, 34, 35], and where the $\ell = 2^{(+)}$ mode $(\tilde{C}_2 > 0)$ is selected as is seen from the criterion (4.15).
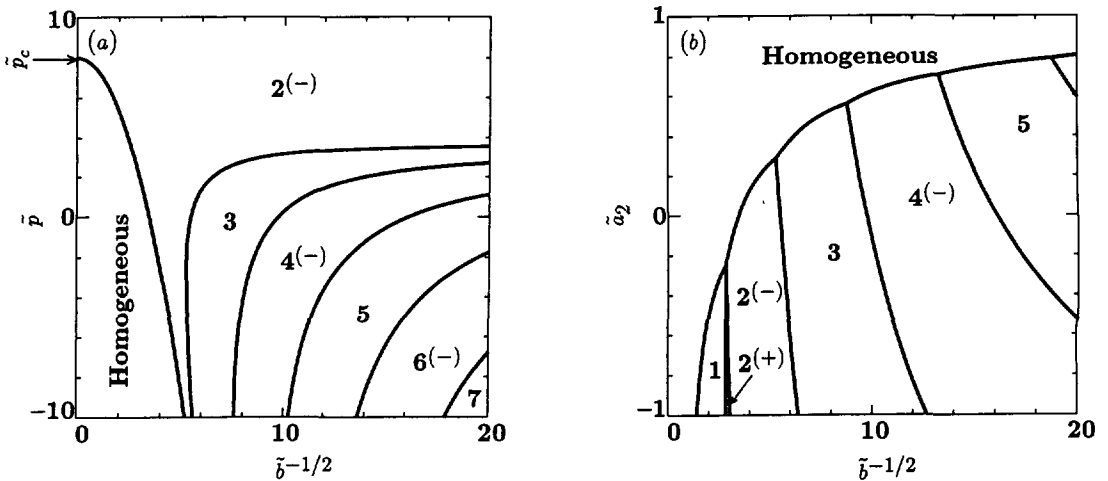

Fig. 6. — Same as figure 5 but for $\tilde{H}_{sp} = -2.0$. All other parameters are the same as those used in figure 5. For $\tilde{p} \geqslant \tilde{p}_c = 8$, the mode selection is determined by the pressure difference in the same way as single-component vesicles [2-4, 34, 35], and where .the $\ell = 2^{(-)}$ mode $(\tilde{C}_2 < 0)$ is selected as is seen from the criterion (4.15).

When the coupling energy is dominant (i.e., $\tilde{b}^{-1/2} \propto \Lambda$ is sufficiently large), the shape with $\tilde{C}_\ell < 0$ is selected as the equilibrium state. On the other hand, when $\tilde{b}^{-1/2}$ is sufficiently small, the shape with $\tilde{C}_\ell > 0$ is selected. The phase boundary between the states $2^{(+)}$ and $2^{(-)}$ shown in figures 5a, b and 6b is determined by such a mechanism.

In figures 5b and 6b, one finds that the shift of critical temperature depends on $\tilde{b}^{-1/2}$ [9, 11] as well as for 2d vesicles. Such a shift of critical temperature is induced by the coupling between the shape and the order parameter. It should be noted that shapes with modes $\ell \geq 2$ are selected even if there is no pressure difference [Figs. 5b and 6b], in contrast to the 2d case where only $n = 2$ is selected without an imposed pressure difference.

5. Concluding remarks.

For two-component vesicles embedded in two and three dimensions, we investigate shape deformations in the vicinity of the bare critical temperature by linear stability analysis. Furthermore, phase diagrams are calculated for 2d vesicles and 3d axisymmetric vesicles using the single mode approximation. The equilibrium shape deformations are mainly determined by the competition between the domain boundary energy and the coupling energy. The domain boundary energy prefers lower modes in order to reduce the domain boundary, and the coupling term prefers higher ones. Therefore, the higher mode selected as the effective coupling coefficient $\tilde{b}^{-1/2}$ becomes large. The selected mode of the shape deformation as well as the order parameter are functions of the pressure difference $\tilde{p}$, temperature $\tilde{a}_2(T)$ and the averaged spontaneous curvature $\tilde{H}_{\mathrm{sp}}$. It is found that the bare critical temperature T_{c}^0 of the phase separation is shifted to a new T_{c}, due to the coupling between the vesicle shape and the order parameter [9, 11]. The phase diagrams obtained in the present work are in qualitative agreement with those obtained for strong segregation limit (low temperatures) presented in our preceding paper [12]. The importance of the domain boundary in determining equilibrium shape deformations of 3d vesicles, such as domain-induced budding [16, 17], is consistent with our result.

Furthermore, we emphasize that the local spontaneous curvature also plays an important role in equilibrium shape deformations [8-15]. In fact, echinocytosis (or crenation) and invagination of red blood cells are induced by intercalation of anionic and cationic amphiphiles into membranes [21]. The origin of such shape deformations seems to be the local asymmetric distribution of amphiphiles between the inner and the outer layers of the membrane [20, 22]. Although we studied the equilibrium shape deformations for 3d axisymmetric vesicles, we expect that shape deformations such as echinocytosis and invagination will be selected as equilibrium states if a shape deformation without the axisymmetry restriction are considered. Further studies of equilibrium shapes without such an axisymmetry restriction is rather mathematically complex and quite challenging.

As another interesting problem, we mention the dynamics of shape deformations of fluid membranes in relation to lateral (intramembrane) spinodal decomposition. The hydrodynamic interaction with the surrounding solvent and a hydrodynamic transport of amphiphiles within fluid membranes have to be included in the dynamics [18]. We hope that in the future controlled experiments on two-component vesicles will become available and will enable a comparison between experiments and theory.

Equilibrium states of single-component vesicles in 3d are also investigated using a single mode approximation. The explicit expansion of the free energy $F_{\mathrm{s}} = F + PV$ for any ℓ-mode is obtained up to the 6th order in $\tilde{C}_\ell$. Using the free energy expansion, free energy branches can be obtained for any general ℓ-mode. The free energy branches for the particular value of

$\ell = 2$ are shown as a function of the pressure $\tilde{p}$ for $\tilde{H}_{sp} = 0$ and -2. The result for zero spontaneous curvature is in qualitative agreement with previous results obtained using a somewhat different variational method [3]. We also obtain the critical spontaneous curvature $\tilde{H}_{sp}^c(\ell)$ which determines the selection between prolate and oblate shapes with a single ℓ mode (ℓ is even). This result is an extension of critical spontaneous curvature obtained for $\ell = 2$, $\tilde{H}_{sp}^c = -1.2$, [4, 33, 35] to any general ℓ mode.

Acknowledgments.

Appendix A.

On the mathematical treatment of membranes.

In this Appendix, we describe the mathematical treatment of membranes. The membrane is regarded as a sheet of vanishing thickness, on which the order parameter field Ψ, such as the relative composition of two kinds of amphiphiles, is defined.

Any point $\mathbf{r}$ belonging to the membrane embedded in a 3d space can be parametrized by any two independent variables u^1 and u^2 as $\mathbf{r}(u^1, u^2)$. The tangential vector along the u^α-direction is given by $\mathbf{g}_\alpha = \mathbf{r}_{,\alpha}$ where the Greek indices stand for 1 or 2 and $X_{,\alpha}$ denotes a partial derivative of X with respect to the variable u^α. The covariant metric tensor $g_{\alpha\beta}$ is provided by $g_{\alpha\beta} = \mathbf{g}_\alpha \cdot \mathbf{g}_\beta$. The normal unit vector $\hat{\mathbf{n}}$ to the surface is obtained by $\hat{\mathbf{n}} = (\mathbf{g}_1 \times \mathbf{g}_2)/\sqrt{g}$ where g is defined by $g = \det(g_{\alpha\beta})$. The contravariant metric tensor is given by the inverse of $g_{\alpha\beta}$. Therefore, satisfying the relation $g_{\alpha\beta} g^{\beta\gamma} = \delta_\alpha^\gamma$, where repeated indices are summed over 1 and 2 and δ_α^β stands for Kronecker's delta function. The contravariant tangential vector is then given by $\mathbf{g}^\alpha = g^{\alpha\beta} \mathbf{g}_\beta$. The tensor $b_{\alpha\beta}$ is defined as $b_{\alpha\beta} = -\mathbf{g}_{\alpha,\beta} \cdot \hat{\mathbf{n}} = \hat{\mathbf{n}}_{,\alpha} \cdot \mathbf{g}_\beta = b_{\beta\alpha}$. The trace and determinant of the tensor b_α^β are two important invariants

$$H = \mathrm{Tr}\,(b_\alpha^\beta) = b_\alpha^\alpha \qquad K = \det\,(b_\alpha^\beta) \tag{A.1}$$

where $\frac{1}{2} H$ is the mean curvature and K is the Gaussian one.

Since the order parameter Ψ is defined only on the surface, its spatial variation $\nabla\Psi$ can be expressed as

$$\nabla\Psi = \Psi_{,\alpha} \mathbf{g}^\alpha \tag{A.2}$$

(a) 2d vesicles. — A 2d vesicle can be regarded as a special case of a 3d vesicle. Namely, the 2d vesicle can be thought of as a cross section of a cylindrical sheet with translational symmetry along one spatial direction (say the z-axis). Using the polar coordinate in the xy-plane, a position on the vesicle is specified by $\mathbf{r}(\theta) = r(\theta)\,\mathbf{e}_r$ where $\mathbf{e}_r$ denotes the unit radius vector (see Fig. 1). The curvature $H = b_\theta^\theta$ is expressed as

$$H = \frac{2\,\dot{r}^2 + r^2 - r\ddot{r}}{(\dot{r}^2 + r^2)^{3/2}} \tag{A.3}$$

where we adopt the notation $\dot{r} = r_{,\theta}$ and $\ddot{r} = r_{,\theta,\theta}$ for clarity purpose and choose the sign of the curvature H to be positive when the vesicle is convex towards the outside region. The total area enclosed by the vesicle is given by

$$A = \frac{1}{2} \int_0^{2\pi} r^2 \, \mathrm{d}\theta \ . \tag{A.4}$$

For 2d vesicles, the identity (2.13) holds for simply-connected (circle-like) shapes as follows

$$\int H \sqrt{g} \, \mathrm{d}u = \int \dot{\Theta}(s) \, \mathrm{d}s = \Theta(s)|_{s=0}^{s=L} = 2\pi \tag{A.5}$$

where $H = \dot{\Theta}(s) \equiv \mathrm{d}\Theta(s)/\mathrm{d}s$, $\mathrm{d}s = \sqrt{g} \, \mathrm{d}u$ and $\Theta(s)$ is the angle between the x-axis and the tangential vector to the contour at the point specified by contour length s (see Fig. 1).

(b) 3d vesicles. — A 3d vesicle with the spherical topology can be parametrized by the two polar angles $(u^1, u^2) = (\theta, \varphi)$. A position on the membrane is specified by the vector $\mathbf{r} = r(\theta, \varphi) \, \mathbf{e}_r$ where $\mathbf{e}_r$ is the unit vector and r is the radius. The area element $\sqrt{g}$ is expressed as

$$\sqrt{g} = \left[r^2 \left((r^2 + r^2_\theta) \sin^2\theta + r^2_\varphi \right) \right]^{1/2} \tag{A.6}$$

Using equations (A.1), the curvature H is

$$H = \frac{r^2 \sin^3\theta}{g^{3/2}} \left[2 r^3 - r^2 A + 3 rB - \left(r^2_{,\theta} A + r_{,\theta\theta} B - r_{,\theta} B_{,\theta} \right) \right] \tag{A.7}$$

where

$$A \equiv r_{,\theta\theta} + \frac{r_{,\varphi\varphi}}{\sin^2\theta} + \frac{\cos\theta}{\sin\theta} r_{,\theta} \qquad B \equiv r^2_{,\theta} + \frac{r^2_{,\varphi}}{\sin^2\theta} \tag{A.8}$$

Using the covariant tangential vectors, the volume inside the vesicle is given by

$$V = \frac{1}{3} \int (\mathbf{g}_\theta \times \mathbf{g}_\varphi) \cdot \mathbf{r} \, \mathrm{d}\theta \, \mathrm{d}\varphi = \frac{1}{3} \int r^3 \sin\theta \, \mathrm{d}\theta \, \mathrm{d}\varphi \ . \tag{A.9}$$

The gradient term $(\nabla\Psi)^2$ in F_2 is expressed as

$$(\nabla\Psi)^2 = \frac{1}{g} \left[r^2 (\Psi^2_{,\theta} \sin^2\theta + \Psi^2_{,\varphi}) + (\Psi_{,\theta} r_{,\varphi} - \Psi_{,\varphi} r_{,\theta})^2 \right]. \tag{A.10}$$

Appendix B.

Free energy for 2d vesicles.

We present detailed expressions for each term in the total free energy using the single mode approximation (SMA). In the linear stability analysis using Fourier expansion of R and Ψ in equations (3.3) and (3.4), it is enough to retain terms up to 2nd order in both $\tilde{c}_n$ $(\tilde{s}_n)$ and $\tilde{\Psi}_{cn}$ $(\tilde{\Psi}_{sn})$. On the other hand, when we study equilibrium states of the vesicle, the equilibrium state is assumed to be a state with a single mode in the Fourier expansion [39]. In order to determine the free energy minimum, terms up to 6th order in $\tilde{c}_n$ and $\tilde{\Psi}_n$ are needed as is mentioned in section 3.2.

Since we assume that the total contour length of the 2d vesicle is constant, c_0 is determined by the constraint (2.4). Expanding the line element in powers of $R(\theta)$ ($|R(\theta)| \ll r_0$), we obtain the following relations

$$\tilde{c}_0 = -\frac{1}{4} n^2 \tilde{c}_n^2 - \frac{1}{64} n^2 (n^2 + 4) \tilde{c}_n^4 - \frac{1}{256} (n^6 + 4 n^4 + 8 n^2) \tilde{c}_n^6 + \cdot \qquad \text{(SMA)} . \quad \text{(B.1)}$$

The integrand in $\tilde{F}_1$ can also be expanded in $R(\theta)$, and using equation (B.1), the relevant terms in the bending energy $\tilde{F}_1$ is found to be

$$\tilde{F}_1 = \frac{1}{2} (n^2 - 1)^2 \tilde{c}_n^2 + \frac{1}{16} \left(n^6 + \frac{41}{2} n^4 - 23 n^2 + 6 \right) \tilde{c}_n^4$$
$$+ \frac{1}{32} \left(3 n^8 + 22 n^6 + 67 n^4 - 56 n^2 + 10 \right) \tilde{c}_n^6 + \cdot \qquad \text{(SMA)} . \quad \text{(B.2)}$$

Using equations (A.4) and (B.1), the pressure term $\tilde{P} \tilde{A} [\equiv (r_0/\pi \kappa) P A]$ is also expanded in power series in $\tilde{c}_n$

$$\tilde{P} \tilde{A} = \tilde{p} \left[-\frac{1}{2} (n^2 - 1) \tilde{c}_n^2 + \frac{1}{32} n^2 (n^2 - 4) \tilde{c}_n^4 - \frac{1}{16} n^2 \tilde{c}_n^6 + \cdot \quad \right] \qquad \text{(SMA)} \quad \text{(B.3)}$$

where in equation (B.3) and in what follows irrelevant constant terms are neglected. Using equation (3.22) and $\sqrt{g}\, du = ds$, the Ginzburg-Landau free energy term is easily calculated

$$\tilde{F}_2 = \frac{1}{2} \left(\tilde{b} n^2 + \tilde{a}_2 + \frac{\tilde{a}_4}{2} \langle \tilde{\Psi} \rangle^2 \right) \tilde{\Psi}_n^2 + \frac{\tilde{a}_4}{32} \tilde{\Psi}_n^4 . \quad \text{(B.4)}$$

Performing rather tedious calculations, the relevant terms in the coupling energy F_3 turn out to be

$$\tilde{F}_3 = (n^2 - 1) \tilde{c}_n \tilde{\Psi}_n + \frac{1}{16} (n^2 - 1)(n^2 - 2) \tilde{c}_n^3 \tilde{\Psi}_n$$
$$+ \frac{1}{3 \cdot 2^8} (-3 n^6 + 79 n^4 + 24 n^2 - 4) \tilde{c}_n^5 \tilde{\Psi}_n + \cdot \qquad \text{(SMA)} . \quad \text{(B.5)}$$

Appendix C.

Calculation of $F_1 + PV$ for 3d vesicles.

Here we present the detailed expressions of the free energy $\tilde{F}_\backslash \equiv \tilde{F}_1 + \tilde{P} \tilde{V}$. Assuming that the total area of the vesicle in 3d is constant, C_0 is determined by the constraint (2.4), which results in equations (4.3) or (4.12), depending on whether one uses Fourier expansion (4.2) or the SMA [Eq. (4.11)], respectively. In the expression of C_0 in equation (4.12), the α_n's are calculated to be

$$\alpha_3 = 0$$
$$\alpha_4 = \frac{1}{32} \left[-I_4^{(2)}(\ell) + \frac{(\ell(\ell + 1) + 2)^2}{(2\ell + 1)^2} \right]$$
$$\alpha_5 = \frac{1}{16} I_5^{(2)}(\ell)$$
$$\alpha_6 = \frac{1}{64} \left[-6 I_6^{(2)}(\ell) + I_6^{(3)}(\ell) - \frac{3}{2} \frac{\ell(\ell + 1) + 2}{2\ell + 1} I_4^{(2)}(\ell) + \frac{1}{2} \frac{(\ell(\ell + 1) + 2)^3}{(2\ell + 1)^3} \right]$$

$$(C.1)$$

where $I_n^{(m)}(\ell)$ is defined as

$$I_n^{(m)}(\ell) \equiv \int_{-1}^{1} (1 - w^2)^m \left(\frac{dP_\ell(w)}{dw} \right)^{2m} [P_\ell(w)]^{n-2m}\, dw\,. \qquad (C.2)$$

The value of $I_n^{(m)}(\ell)$ can be evaluated analytically because $P_\ell(w)$ is a polynomial function of w, and is non-vanishing only if $\ell \cdot n$ is even. The detailed expression of $W^{(n)}$ in equation (4.13) is given by,

$$W^{(n)}(\ell, \tilde{H}_{\mathrm{sp}}, \tilde{p}) \equiv X_n(\ell) + \tilde{H}_{\mathrm{sp}}\, Y_n(\ell) + \tilde{p} Z_n(\ell) \qquad (C.3)$$

where $X_n(\ell)$, $Y_n(\ell)$ and $Z_n(\ell)$ are defined as

$$\frac{1}{16\pi} \int H^2 \sqrt{g}\, d\theta\, d\varphi \equiv 1 + \sum_{n=2}^{\infty} X_n(\ell)(\tilde{C}_\ell)^n$$

$$-\frac{H_{\mathrm{sp}}}{8\pi} \int H \sqrt{g}\, d\theta\, d\varphi \equiv \tilde{H}_{\mathrm{sp}}\left[-1 + \sum_{n=2}^{\infty} Y_n(\ell)(\tilde{C}_\ell)^n \right] \qquad (C.4)$$

$$\tilde{P}\tilde{V} \equiv \tilde{p}\left[\frac{1}{3} + \sum_{n=2}^{\infty} Z_n(\ell)(\tilde{C}_\ell)^n \right].$$

In order to evaluate the energy minima of $\tilde{F}_s$, the coefficient of the highest order term in $\tilde{C}_\ell$ must be positive. As the coefficient $X_4(\ell)$ is negative for $\ell \geq 3$, we must take into account terms up to 6th order in $\tilde{C}_\ell$, where the coefficient of $(\tilde{C}_\ell)^6$ in $\tilde{F}_s$, i.e., $W^{(6)}(\ell, \tilde{H}_{\mathrm{sp}}, \tilde{p})$, is positive definite for any ℓ (except for unphysically large values of $|\tilde{H}_{\mathrm{sp}}|$ and $|\tilde{p}|$). Therefore, we calculate terms up to the 6th order in $\tilde{C}_\ell$ in $\tilde{F}_s$. The explicit expressions of $X_n(\ell)$, $Y_n(\ell)$ and $Z_n(\ell)$ for $n = 4$, 5 and 6 are given as follows

$$X_4(\ell) \equiv \frac{1}{16}\left[\left(\frac{1}{3}\ell^3(\ell+1)^3 + 2\,\ell^2(\ell+1)^2 - 4\,\ell(\ell+1) \right) I_4^{(0)}(\ell) \right.$$

$$\left. + \left(-2\,\ell(\ell+1) + 5 \right) I_4^{(2)}(\ell) + 2\frac{\ell^3(\ell+1)^3 - 4\,\ell(\ell+1)}{(2\,\ell+1)^2} \right]$$

$$X_5(\ell) \equiv \frac{1}{32}\left[-2\left(\ell^3(\ell+1)^3 + 2\,\ell^2(\ell+1)^2 - 4\,\ell(\ell+1) \right) I_5^{(0)}(\ell) \right.$$

$$\left. + 2\left(11\,\ell(\ell+1) - 20 \right) I_5^{(2)}(\ell) - 3\frac{\ell^3(\ell+1)^3 - 4\,\ell(\ell+1)}{2\,\ell+1} I_3^{(0)}(\ell) \right]$$

$$X_6(\ell) = \frac{1}{64}\left[8\left(\ell^3(\ell+1)^3 + \ell^2(\ell+1)^2 - 2\,\ell(\ell+1) \right) I_6^{(0)}(\ell) \right.$$

$$+ 5\left(-\ell^2(\ell+1)^2 - 28\,\ell(\ell+1) + 40 \right) I_6^{(2)}(\ell) + 2\left(4\,\ell(\ell+1) - \frac{17}{3} \right) I_6^{(3)}(\ell)$$

$$+ 4\frac{\ell(\ell+1) + 2}{2\,\ell+1}\left(\frac{1}{3}\ell^3(\ell+1)^3 + 2\,\ell^2(\ell+1)^2 - 4\,\ell(\ell+1) \right) I_4^{(0)}(\ell)$$

$$+ \frac{1}{2\,\ell+1}\left(-9\,\ell^2(\ell+1)^2 + 6\,\ell(\ell+1) + 40 \right) I_4^{(2)}(\ell)$$

$$\left. + \frac{4\,\ell(\ell+1)}{(2\,\ell+1)^3}\left(\ell(\ell+1) - 2 \right)\left(\ell(\ell+1) + 2 \right)^2 \right] \qquad (C.5)$$

$$Y_4(\ell) = \frac{1}{16} \left[\frac{4}{3} \left(\ell^2(\ell+1)^2 - \ell(\ell+1) \right) I_4^{(0)}(\ell) - \frac{1}{2} I_4^{(2)}(\ell) \right.$$

$$\left. - \frac{1}{2(2\ell+1)^2} \left(\ell(\ell+1)+2 \right) \left(3\ell(\ell+1)-2 \right) \right]$$

$$Y_5(\ell) = \frac{1}{32} \left[\left(-3\ell^2(\ell+1)^2 + 2\ell(\ell+1) \right) I_5^{(0)}(\ell) + 2 \left(\ell(\ell+1)+1 \right) I_5^{(2)}(\ell) \right.$$

$$\left. - \frac{1}{2\ell+1} \left(\ell^3(\ell+1)^3 - 4\ell(\ell+1) \right) I_5^{(0)}(\ell) \right]$$

$$Y_6(\ell) = \frac{1}{64} \left[\frac{16}{5} \left(2\ell^2(\ell+1)^2 - \ell(\ell+1) \right) I_6^{(0)}(\ell) - 2 \left(8\ell(\ell+1)+3 \right) I_6^{(2)}(\ell) \right.$$

$$+ I_6^{(3)}(\ell) + 4\frac{\ell(\ell+1)}{2\ell+1} \left(\ell(\ell+1)-1 \right) \left(\ell(\ell+1)+2 \right) I_4^{(0)}(\ell)$$

$$- \frac{1}{2(2\ell+1)} \left(\ell(\ell+1)+6 \right) I_4^{(2)}(\ell)$$

$$\left. - \frac{1}{2(2\ell+1)^3} \left(\ell(\ell+1)+2 \right)^2 \left(5\ell(\ell+1)-2 \right) \right] \tag{C.6}$$

$$Z_4(\ell) = \frac{1}{16} \left[\frac{1}{2} I_4^{(2)}(\ell) + \frac{1}{2(2\ell+1)^2} \left(\ell(\ell+1)-6 \right) \left(\ell(\ell+1)+2 \right) \right]$$

$$Z_5(\ell) = \frac{1}{32} \left[-2 I_5^{(2)}(\ell) \right]$$

$$Z_6(\ell) = \frac{1}{64} \left[6 I_6^{(2)}(\ell) - I_6^{(3)}(\ell) + \frac{1}{2(2\ell+1)} \left(\ell(\ell+1)+6 \right) I_4^{(2)}(\ell) \right.$$

$$\left. + \frac{1}{6(2\ell+1)^3} \left(\ell(\ell+1)+2 \right)^2 \left(\ell(\ell+1)-10 \right) \right]. \tag{C.7}$$

Appendix D.

Remarks on the order parameter in SMA.

In order to explore phase diagrams using the single mode approximation, extra care should be given to the precise definition of the order parameter for the SMA.

(a) 2d *vesicles*. — The L-periodic function of the natural coordinate s with a single n mode [see Eq. (3.22)] is used for the investigation of phase diagrams in section 3.2. The reason is as follows.

If one uses the form

$$\Psi = \psi_0 + \sum_{n=1}^{\infty} \left\{ \psi_{cn} \cos n\theta + \psi_{sn} \sin n\theta \right\}, \tag{D.1}$$

where

$$\psi_0 = \langle \Psi \rangle - \frac{1}{2r_0} \sum_{n=1}^{\infty} (c_n \psi_{cn} + s_n \psi_{sn}) + \cdot \quad , \qquad \langle \Psi \rangle \equiv \frac{M}{2\pi r_0} \tag{D.2}$$

the result of the linear stability analysis is same as that obtained by the expansion (3.4). Namely, there is no difference in the choice of bases of the expansion as long as one only performs a linear stability analysis.

However, since we used a single mode approximation to study phase diagrams as is described in section 3.2, the choice of bases for the expansion of Ψ becomes a crucial point. If one uses the order parameter specified by a single mode of the expansion of equation (D.1),

$$\Psi = \psi_0 + \psi_n \cos n\theta \qquad \psi_0 = \langle \Psi \rangle - \frac{1}{2\,r_0}\,c_n\,\psi_n + \cdot \qquad (n \neq 0) \qquad (D.3)$$

the order parameter profile along the contour s is changed by the shape deformation. This change of the order parameter profile can be seen, if a ring vesicle is expanded to a straight line while keeping the total contour length and profiles of Ψ for different c_n but with fixed n and ψ_n are compared. This change comes from the change of the line element $\sqrt{g(\theta)}$ due to shape deformations. Namely, the order parameter profile is not specified by n and ψ_n alone in this case. Using this order parameter of equation (D.3), it is not clear how to describe the state of the order parameter with a single n mode. Therefore, the use of equation (D.1) as a single mode state is not suitable in SMA.

On the other hand, if equation (3.22) is used as the order parameter in SMA,

$$\Psi = \Psi_0 + \Psi_n \cos \frac{2\pi n}{L}\,s \quad \text{where} \quad \Psi_0 = \langle \Psi \rangle \qquad (D.4)$$

the order parameter profile does not depend on the vesicle shape because of $\sqrt{g} = 1$, and is suitable to study phase diagrams in SMA. Accordingly, the expansion (3.4) and its single mode (3.22) are used.

(b) 3d vesicles. — For an axisymmetric 3d vesicle, a possible selection of the order parameter with a single ℓ mode ($m = 0$) is that of equation (4.2),

$$\Psi(\theta) = \psi_0 + \psi_\ell\,P_\ell(\cos \theta)\,, \qquad \psi_\ell \equiv \psi_{\ell 0}\,N_{\ell 0} \quad (\ell \neq 0) \qquad (D.5)$$

where ψ_0 is determined by the constraint (2.8)

$$\psi_0 = \langle \Psi \rangle - \frac{2}{2\,\ell + 1}\,\tilde{C}_\ell\,\psi_\ell + \cdot \quad , \qquad \langle \Psi \rangle \equiv \frac{M}{4\,\pi r_0^2}\,. \qquad (D.6)$$

Here we use a lower case notation for the coefficients ψ's in order to distinguish them from that of equation (4.2). Since the order parameter of equation (D.5) is given in the θ-space, equation (D.5) is not suitable to investigate equilibrium states in SMA for the same reasons as was explained above for 2d. When the order parameter with a single mode is given, the change of the area element $\sqrt{g(\theta)}$ due to the shape deformation should be taken into account like in the 2d case.

The order parameter $\Psi(\theta)$ on a *deformed* vesicle with a single ℓ mode is given by the following procedure. First (see Fig. 7a) the order parameter $\Psi'(\theta')$ with a single mode ℓ is given on the *perfect sphere* (before the shape deformation) as

$$\Psi'(\theta') = \Psi_0 + \Psi_\ell\,P_\ell(\cos \theta') \qquad (\ell \neq 0) \qquad (D.7)$$

where θ' denotes the polar angle specifying a position of a infinitesimal area dS' on the sphere, in which the value of the order parameter is assumed to be constant $\Psi'(\theta')$. After the shape deformation, the area dS' changes into a deformed area dS, in which the value of the order parameter, $\Psi(\theta)$, is assumed to be the same as $\Psi'(\theta')$ in dS'. Thus, the order parameter after the shape deformation is given by

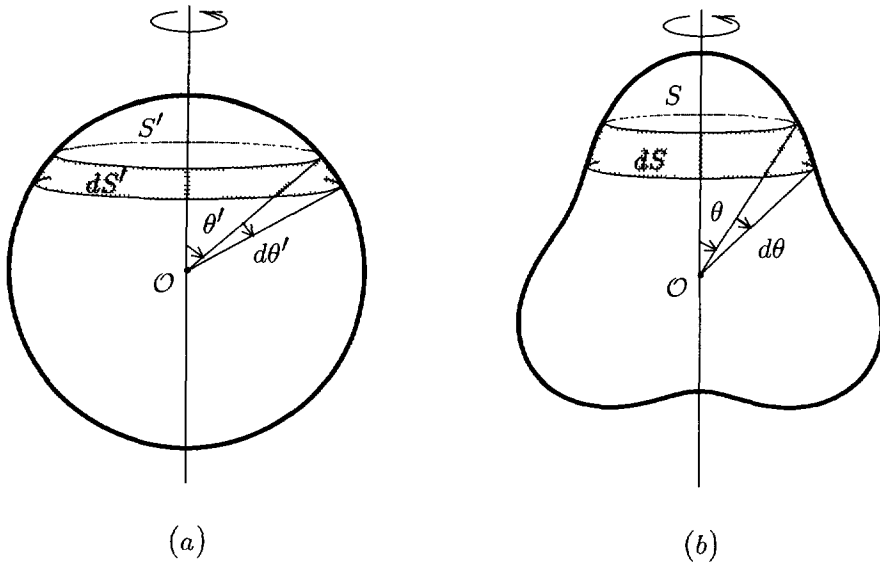$$\Psi[\theta(\theta')] = \Psi'(\theta') \qquad (D.8)$$

Fig. 7. — Schematic representation showing how an infinitesiaml ring-like area dS' on a perfect sphere is mapped onto a deformed surface through a shape deformation. (a) An order parameter with an ℓ mode is defined on a perfect spherical shape (before the shape deformation). The order parameter is given by $\Psi'(\theta')$ at the area dS' specified by a polar angle θ'. (b) After a shape deformation with the same ℓ mode, the area dS' is mapped onto dS specified by θ, while keeping its area fixed. From the mapping, a mapping function $\theta(\theta')$ and an order parameter profile after the shape deformation $\Psi(\theta) = \Psi'[\theta'(\theta)]$ are obtained.

where θ denotes the polar angle specifying the position of the area dS [see Fig. 7b]. The mapping from θ' to θ is determined by the constraint that the local area of the membrane is unstretchable. However, the shape of a piece of the membrane can be deformed due to the fluidity of the amphiphilic sheet. Since the local area of the membrane is unchanged by the shape deformation (i.e., $dS' = dS$), the following relation is obtained (see Figs. 7a and b)

$$r_0^2 \sin \theta' \, d\theta' = \sqrt{g} \, d\theta \qquad (D.9)$$

or equivalently

$$\int_0^{\theta'} r_0^2 \sin \theta'' \, d\theta'' = \int_0^{\theta} \sqrt{g(\theta'')} \, d\theta'' \qquad (D.10)$$

In this formalism, Ψ_0 is exactly the average of the order parameter irrespective of the shape deformation, which is different from equation (4.4). Actually, using equations (2.8), (D.7) and (D.8), Ψ_0 is found to be

$$\int \Psi(\theta) \sqrt{g} \, d\theta \, d\varphi = \int \Psi'(\theta') r_0^2 \sin \theta' \, d\theta' \, d\varphi' = 4\pi r_0^2 \, \Psi_0 = M \,. \qquad (D.11)$$

The constraint (2.8) is always satisfied by taking Ψ_0 as

$$\Psi_0 = \langle \Psi \rangle \,. \qquad (D.12)$$

Using equations (D.7-D.9), the gradient term in F_2 is expressed as

$$\int \sqrt{g}\,[\nabla \Psi(\theta)]^2 \, d\theta \, d\varphi = \int \sqrt{g}\,[\nabla \Psi'(\theta'(\theta))]^2 \, d\theta \, d\varphi$$

$$= 2\pi \Psi_\ell^2 \int_{-1}^{1} r\left[r^2 + (1 - w^2)\left(\frac{dR}{dw}\right)^2\right]^{-1/2}$$

$$\times (1 - w^2)\left[\frac{d}{dw'} P_\ell(w')\right]^2 dw \qquad (D.13)$$

where $w \equiv \cos\theta$ and $w' \equiv \cos\theta'$. We can obtain a relation between w and w' by expanding $\sqrt{g}$ in equation (D.10) in powers of the small deviation R,

$$w' = w + \int_1^{w'}\left[\frac{2}{r_0}R + \frac{1}{2\,r_0^2}(2\,R^2 + B) + \cdot\right] dw'' \qquad (D.14)$$

Using equation (D.14), the gradient term is expanded as a power series in $\tilde{C}_\ell$. The expression of $G_4(\ell)$ in equation (4.16) is then found to be

$$G_4(\ell) = \frac{\ell^2(\ell + 1)^2 + 2\,\ell(\ell + 1)}{2(2\,\ell + 1)^2} - \frac{1}{12}\,\ell(\ell + 1)(\ell(\ell + 1) + 6)\,I_4^{(0)}(\ell)$$

$$- \frac{1}{4\,\ell^2(\ell + 1)^2}\left(\ell^2(\ell + 1)^2 - 8\,\ell(\ell + 1) + 8\right)I_4^{(2)}(\ell)\,. \qquad (D.15)$$

In a similar fashion, the coupling energy is

$$F_3 = \Lambda \int H\,\Delta\Psi(\theta)\,\sqrt{g}\,d\theta\,d\varphi = \Lambda \int H\,\Delta\Psi'(\theta'(\theta))\,\sqrt{g}\,d\theta\,d\varphi\,. \qquad (D.16)$$

Using equations (D.7), (D.8) and (D.10), the coupling energy $\tilde{F}_3$ results in equation (4.18) by a straightforward but tedious calculation. The explicit expression of $S_4(\ell)$ in equation (4.18) turns out to be

$$S_4(\ell) = \frac{1}{48}\left(\ell^2(\ell + 1)^2 + 8\,\ell(\ell + 1) - 4\right)I_4^{(0)}(\ell)$$

$$- \frac{1}{8\,\ell^2(\ell + 1)^2}\left(\ell^2(\ell + 1)^2 + 4\,\ell(\ell + 1) - 8\right)I_4^{(2)}(\ell)$$

$$+ \frac{1}{8(2\,\ell + 1)^2}\left(\ell^2(\ell + 1)^2 - 4\right)\,. \qquad (D.17)$$

We also calculated G_n and S_n for $n = 5$ and 6 and confirmed that these terms give insignificant contributions to the phase diagram.

References

[1] Canham P. B., *J. Theor. Biol.* **26** (1970) 61 ;
   Helfrich W., *Z. Naturforsch.* **28c** (1973) 693.
[2] Deuling H. J. and Helfrich W., *J. Phys. France* **37** (1976) 1335 ; *Biophys. J.* **16** (1976) 861.
[3] Jenkins J. T., *J. Math. Biol.* **4** (1976) 149.

[4] Seifert U., Berndl K. and Lipowsky R., *Phys. Rev. A* **44** (1991) 1182.

[5] MacKintosh F. C. and Lubensky T. C., *Phys. Rev. Lett.* **67** (1991) 1169 ;
Lubensky T. C. and MacKintosh F. C., *Phys. Rev. Lett.* **71** (1993) 1565.

[6] Boal D. H., Seifert U. and Zilker A., *Phys. Rev. Lett.* **69** (1992) 3405.

[7] Kodama H. and Komura S., *J. Phys. II France* **3** (1993) 1305.

[8] Leibler S., *J. Phys. France* **47** (1986) 507.

[9] Leibler S. and Andelman D., *J. Phys. France* **48** (1987) 2013.

[10] Andelman D., Kawakatsu T. and Kawasaki K., *Europhys. Lett.* **19** (1992) 57.

[11] Taniguchi T., Kawasaki K., Andelman D. and Kawakatsu T., *Cond. Matt. Mater. Commun.* **1** (1993) 75.

[12] Kawakatsu T., Andelman D., Kawasaki K. and Taniguchi T., *J. Phys. II France* **3** (1993) 971.

[13] Safran S. A., Pincus P. A. and Andelman D., *Science* **248** (1990) 354 ;
Safran S. A., Pincus P. A., Andelman D. and MacKintosh F. C., *Phys. Rev. A* **43** (1991) 1071.

[14] MacKintosh F. C. and Safran S. A., *Phys. Rev. E* **47** (1993) 1180.

[15] Seifert U., *Phys. Rev. Lett.* **70** (1993) 1335.

[16] Lipowsky R., *J. Phys. II France* **2** (1992) 1825.

[17] Jülicher F. and Lipowsky R., *Phys. Rev. Lett.* **70** (1993) 2964.

[18] Onuki A., *J. Phys. Soc. Jpn* **62** (1993) 385.

[19] Morikawa R. and Saito Y., *J. Phys. II France* **4** (1994) 145.

[20] Gebhardt C., Gruler H. and Sackmann E., *Z. Naturforsch.* **32c** (1977) 581 ;
Sackmann E., Rüppel D. and Gebhardt C., Liquid Crystals of One and Two Dimensional Order, W. Helfrich and G. Heppke Eds. (Springer-Verlag, Berlin 1980).

[21] Deuticke B., *Biochim. Biophys. Acta* **163** (1968) 494.

[22] Sheetz M. P. and Singer S. J., *Proc. Nat. Acad. Sci. USA* **74** (1974) 4475 ;
Sheetz M. P., Painter R. G. and Singer S. J., *J. Cell Biol.* **70** (1976) 193.

[23] Vesicles with nonzero genus (e.g. toroidal vesicles) have been observed experimentally. See for example : Mutz M. and Bensimon D., *Phys. Rev. A* **43** (1991) 4525 ;
Fourcade B., Mutz M. and Bensimon D., *Phys. Rev. Lett.* **68** (1992) 2551.

[24] In the case where an amphiphilic monolayer consists of one type of amphiphiles with a difference in sizes between the polar head and hydrocarbon tail (e.g., the shape of an amphiphilic molecule is just like a wedge), a spontaneous curvature may be introduced into the bending energy in equation (2.1). Such a term also enters into the total free energy through the coupling energy F_3 [see Eqs. (2.10) and (2.11)].

[25] We consider a vesicle which is made out of two kinds of amphiphiles, where the elastic modulus may depend, in general, on the total composition of the membrane. However, for simplicity, we neglected such a composition dependence of the elastic modulus.

[26] Coxeter H. S. M., Introduction to Geometry (J. Wiley, New York, 1965) ;
Visconti A., Introductory Differential Geometry for Physicists (World Scientific, Singapore, 1992).

[27] Kornberg R. D. and McConnell H. M., *Biochem.* **10** (1971) 1111.

[28] Petrov A. G. and Bivas J., *Prog. Surf. Sci.* **16** (1984) 389.

[29] Seifert U., *Phys. Rev. A* **43** (1991) 6803.

[30] Peterson M. A., *Phys. Rev. Lett.* **61** (1988) 1325 ;
Ou-Yang Zhong-can and Helfrich W., *Phys. Rev. Lett.* **61** (1988) 1326.

[31] Neglecting higher than 2nd order terms for $\tilde{p} < \tilde{p}_c = 3$ was checked numerically by taking into account higher order terms in $\tilde{c}_n$ and $\tilde{\Psi}_n$ up to 6th order. Indeed, the resulting phase diagrams do not depend in any significant way on the 3rd and 4th order terms in $\tilde{c}_n$ and can be omitted when $\tilde{p} < 3$.

[32] Further increase in the external pressure leads to unphysical situation where the vesicle will intersect itself in an unphysical way. For example, a single-component vesicle on the $n = 2$ branch self-intersects at a pressure $\tilde{p} = 5.4$ as is explained in reference [29].

[33] See e.g., Milner S. T. and Safran S. A., *Phys. Rev. A* **36** (1987) 4371.

[34] Ou-Yang Zhong-can and Helfrich W., *Phys. Rev. Lett.* **59** (1987) 2486.

[35] Ou-Yang Zhong-can and Helfrich W., *Phys. Rev. A* **39** (1989) 5280.

[36] Landau L. D. and Lifshitz E. M., Quantum Mechanics (Pergamon, New York, 1977).

[37] In another approach, the threshold value of the spontaneous curvature (the critical spontaneous curvature) $\tilde{H}_{sp} > - 39/23$ is obtained by Deuling and Helfrich (see Ref. [2]). They evaluated this threshold value using a perturbative method. The difference in the two values of the critical spontaneous curvatures is discussed by Peterson M. A., *J. Appl. Phys.* **57** (1985) 1739.

[38] For $\tilde{H}_{sp} = 0$, Jenkins used a somewhat different method and obtained such a first-order phase transition for $\tilde{p}_1 = 5.69$ and the appearance of a metastable state at $\tilde{p}_2 = 5.64$. These values are evaluated numerically by solving the *Euler-Lagrange* equation for the axisymmetric case. For more details (see Ref. [3]). Our obtained values for $\tilde{p}_1$ and $\tilde{p}_2$ are different from Jenkins's, the difference comes from the single mode approximation and the truncation of the free energy expansion.

[39] The superposition of $c_n \cos n\theta$ and $s_n \sin n\theta$, expressing a vesicle shape, can be expressed by $\sqrt{c_n^2 + s_n^2} \cos (n\theta + \delta)$, δ being a phase shift. The order parameter is also expressed by $\sqrt{\Psi_{c,n}^2 + \Psi_{s,n}^2} \cos \left(\dfrac{2 \pi n}{L} s(\theta) + \delta' \right)$, δ' being phase shift. We use equations (3.21) and (3.22) in SMA, because a coherent state $(\delta = \delta')$ of the shape and the order parameter is energetically lower than other incoherent states due to the coupling term F_3.